

Astrophysical Conditions for Planetary Habitability

Manuel Güdel, Rudolf Dvorak

University of Vienna

Nikolai Erkaev

Russian Academy of Sciences

James Kasting

Penn State University

Maxim Khodachenko, Helmut Lammer

Austrian Academy of Sciences

Elke Pilat-Lohinger

University of Vienna

Heike Rauer

Deutsches Zentrum für Luft- und Raumfahrt (DLR) and TU Berlin

Ignasi Ribas

Institut d'Estudis Espacials de Catalunya - CSIC

Brian E. Wood

Naval Research Laboratory

With the discovery of hundreds of exoplanets and a potentially huge number of Earth-like planets waiting to be discovered, the conditions for their habitability have become a focal point in exoplanetary research. The classical picture of habitable zones primarily relies on the stellar flux allowing liquid water to exist on the surface of an Earth-like planet with a suitable atmosphere. However, numerous further stellar and planetary properties constrain habitability. Apart from "geophysical" processes depending on the internal structure and composition of a planet, a complex array of astrophysical factors additionally determine habitability. Among these, variable stellar UV, EUV, and X-ray radiation, stellar and interplanetary magnetic fields, ionized winds, and energetic particles control the constitution of upper planetary atmospheres and their physical and chemical evolution. Short- and long-term stellar variability necessitates full time-dependent studies to understand planetary habitability at any point in time. Furthermore, dynamical effects in planetary systems and transport of water to Earth-like planets set fundamentally important constraints. We will review these astrophysical conditions for habitability under the crucial aspects of the long-term evolution of stellar properties, the consequent extreme conditions in the early evolutionary phase of planetary systems, and the important interplay between properties of the host star and its planets.

1. INTRODUCTION

Discovery of planets around other stars is now well underway. Over 1000 extrasolar planets have been found mainly by ground-based radial velocity (RV) measurements and space- and ground-based photometric transit surveys (exoplanets.org). In addition, ≈ 3500 "planet candidates" have been found by Kepler (Batalha *et al.*, 2013; updates as of November 2013). Due to instrument sensitivity the first planets detected were predominantly gas or

ice giants, like Jupiter or Neptune. Recent work by Howard (2013) and Fressin *et al.* (2013) show that small transiting planets are more numerous than big ones. Some potentially rocky planets have been identified (Léger *et al.*, 2009; Batalha *et al.*, 2011, Borucki *et al.*, 2013). Several planets with minimum masses consistent with rocky planets have been found mostly around cooler stars, including planets in the Habitable Zones (Pepe *et al.* 2011; Anglada-Escudé *et al.*, 2012; Bonfils *et al.*, 2013), as these stars are less

massive and smaller, and hence more easily accelerated by small planets, and show an improved planet/star contrast ratio in the photometric transit method. The search is now on for rocky planets around FGKM stars. A handful of these have already been found (*Buchhave et al.*, 2012; see also website exoplanets.org). This search is difficult to do by RV because the induced stellar velocities are small. Kepler can find close-in rocky planets around FGK stars rather easily compared to planets at larger radii. However, small, potentially rocky planets in the habitable zone are difficult to verify, since most of the solar-like stars are noisier than the Sun, and those identified by Kepler are far away, hence dim (*Gilliland et al.*, 2011). Nevertheless, the first few transiting planets with radii consistent with rocky planets have been recently detected in Habitable Zones (*Borucki et al.*, 2013; *Kopparapu*, 2013; *Kaltenegger et al.*, 2013).

In this chapter we are concerned with habitable planets. Below, we expand on what we mean by that term. A fundamental requirement of habitability, though – perhaps the only indisputable requirement – is that the planet must have a solid or liquid surface to provide stable pressure-temperature conditions. In his book *Cosmos*, Carl Sagan imagined hypothetical bag-like creatures that could live on Jupiter by adjusting their height in the atmosphere, just as some fish can adjust their depth in Earth’s oceans using air bladders. But one needs to ask how such creatures might possibly evolve. Single-celled organisms could not maintain their altitude on a gas or ice giant planet, and hence would eventually be wafted up to the very cold (unless it was a hot Jupiter) upper atmosphere or down into the hot interior. Here we assume that Sagan’s gas giant life forms do not exist, and we focus our attention on rocky planets. Habitability for extrasolar planets is usually defined by liquid water on the surface of a rocky planet. Other liquids can be imagined, as discussed below. Furthermore, water may exist also subsurface, as, e.g., expected for Jupiter’s icy moon Europa, which would make such a body also potentially habitable. In terms of exoplanets, however, such sub-surface life would be very difficult to detect, and we neglect it here.

2. WHAT IS HABITABILITY?

To begin, we must define what constitutes a rocky planet. That definition is easy enough if you can characterize the planet the way we do for objects in our own Solar System: it must have a solid or liquid surface. But if one knows only the planet’s minimum mass (from RV) or its diameter (from transits), this question becomes more difficult. Astrophysical theory predicts that planets that grow larger than about 10 Earth masses during the time that the stellar nebula is still around will capture significant amounts of gas and turn into gas or ice giants (*Mizuno et al.*, 1978; *Pollack et al.*, 1996). The theory is not robust, however, because the opacity calculations within the accreting atmosphere are complex and did not include such phenomena as collision-induced absorption of IR radiation by molecular hydrogen,

and because it does not exclude higher-mass planets that complete the process of accretion after the nebular gas has disappeared. Similarly, measurement of a planet’s diameter via the transit method does not distinguish conclusively between a rocky planet like Earth or an ice giant like Neptune. Neptune’s diameter is about 4 times that of Earth. Initial data indicate that planets with radii below $2R_{\text{Earth}}$ are rocky. The Kepler team assumes that planets with diameters $> 2R_{\text{Earth}}$ are ice giants.

Once we are sure that a planet is rocky, the next most fundamental requirement for life as we know it is that it should have access to liquid water. Even though some terrestrial organisms – those that form spores, for example – can persist for long time intervals without water, all terrestrial life forms require liquid water to metabolize and reproduce. There are good biochemical reasons for this dependence. Most importantly, water is a highly polar solvent that can dissolve the polar molecules on which carbon-based life depends. That said, researchers do not completely discount the possibility that alien life forms might have different biochemistries (*Baross et al.*, 2007; *National Academy of Sciences*, 2007). Carbon has a more complex chemistry than any other element, and so most workers agree that alien life would also be carbon-based. Other chain building elements like silicon and phosphorus exist, but are less energetically favorable than C in this respect. Among alternative solvents, even liquid CH_4 is considered by some workers to be a possible medium in which life might exist; hence, the interest in Saturn’s moon Titan, which has lakes of liquid methane on its surface. Liquid methane is only stable at very low temperatures, though, and so any organic chemistry in it may be too slow to create or to power life. We suspect that liquid water, or some mixture containing liquid water, is needed to support all forms of life.

Confining our interest to planets with liquid water is not all that restrictive. Oxygen is the third most abundant element in the universe, and so many, or most, rocky planets are probably endowed with appreciable amounts of water when they form (e.g., *Raymond et al.*, 2007). In our own Solar System, Mercury and Venus lack liquid water, while Earth and Mars have it although modern Mars has no liquid water in amounts sufficient to develop life. The lack of water on the innermost two planets is easily explained, though, as these planets lie outside the boundaries of the habitable zone – the region around a star where liquid water can be present on a planet’s surface (*Hart*, 1979; *Kasting et al.*, 1993). Mars lacks liquid water on its surface today, but shows evidence that water flowed there earlier in its history. And Mars may have liquid water in its subsurface. Mars’ internal heat flow is thought to be about 1/3rd that of Earth (*Montési and Zuber*, 2003); hence, depending on the thermal conductivity of the regolith, Mars could have liquid water within a few kilometers of the surface.

As astronomers, we are interested in discovering life on extrasolar planets. For the foreseeable future, at least, such planets can only be studied remotely, by doing spectroscopy on their atmospheres using big telescopes on the ground or,

more likely, in space. For us to detect life on an exoplanet, that life must be able to modify the planet's atmosphere in such a way that we can detect it, as it has done here on Earth. Earth's atmosphere contains 21% O₂ and 1.7 ppmv CH₄, both of which are produced almost entirely by organisms. The maintenance of extreme disequilibrium in a planet's atmosphere, and specifically the coexistence of free O₂ with reduced gases such as CH₄ or N₂O, was suggested many years ago as the best remote evidence for life (*Lederberg, 1965; Lovelock, 1965*). If we wish to propose a testable hypothesis about life on other planets, we should therefore restrict our attention to planets like Earth that have liquid water on their surfaces. This allows for the possibility that photosynthetic life might flourish there, greatly increasing productivity (*Kharecha et al., 2005*), and possibly producing atmospheric biosignatures that we might one day detect.

From a practical standpoint, then, this means that we should design our astronomical searches to look for planets lying within the conventional liquid water habitable zone (HZ) of their parent star. This is a necessary, but not sufficient, condition, as factors such as volatile inventories, high-energy radiation, magnetospheres, and stellar winds may further constrain habitability, as discussed further in this chapter. The boundaries of the HZ were estimated by *Kasting et al. (1993)* based on 1-D climate modeling calculations for Earth-like planets. These calculations were done with a cloud-free model (clouds were "painted" on the ground) and they assumed fully saturated tropospheres. Conservatively, planets may lose their water when they lie closer to the star than the "moist greenhouse" limit. At this distance, ≈ 0.95 AU in these old calculations, a planet's stratosphere becomes wet, and the water is lost by photodissociation followed by escape of hydrogen to space. A more strict limit of the inner edge of the habitable zone is the so-called runaway greenhouse limit. At this limit the entire water ocean of the Earth would reside within the atmosphere due to the self-enhancing water vapor feedback cycle. The outer edge of the HZ is defined by the "maximum greenhouse" limit, beyond which a CO₂-H₂O greenhouse is no longer capable of maintaining a warm surface. This limit is based on the assumption that an Earth-like planet will have volcanoes that emit CO₂ and that CO₂ will accumulate in the planet's atmosphere as the surface becomes cold. But, at some point, CO₂ will begin to condense out of the planet's atmosphere, limiting the range of distances over which this feedback process works. In these old calculations, the maximum greenhouse limit occurs at ≈ 1.67 AU for our Sun. The "1st CO₂ condensation" limit of *Kasting et al. (1993)* is no longer considered valid, because CO₂ clouds are now thought to usually warm a planet's surface (*Forget and Pierrehumbert, 1997; Mischna et al., 2000*). *Kitzmann et al. (2013)*, however, suggest that the warming effect may have been overestimated in some cases. More optimistic empirical limits on the HZ are derived from the observation that early Mars appears to lie within it, and Venus could conceivably have been within it prior to ≈ 1 billion years ago. An even more optimistic outer edge has been suggested for

the HZ by *Seager (2013)*, based on a calculation by *Pierrehumbert and Gaidos (2011)* showing that super-Earths with dense captured H₂ atmospheres could remain habitable out to as far as 10 AU in our Solar System. Such planets will remain speculative, however, until they are observed, and one would not want to count on their existence while defining the requirements for a telescope to search for extrasolar life (*Kasting et al., 2014*).

Recently, *Kopparapu et al. (2013)* rederived the HZ boundaries using a new 1-D climate model based on the HITEMP database for H₂O. HITEMP differs from the older HITRAN database by including many more weak absorption lines, including some that extend all the way down to near-UV wavelengths. They furthermore included a new formulation of the water vapor continuum by *Paynter and Ramaswamy (2011)*. This causes the albedo of an H₂O-rich atmosphere to be substantially lower than previously calculated. Consequently, the moist greenhouse limit for the inner edge moves out to 0.99 AU (Fig. 1). This does not indicate that Earth is actually that close to it, as these calculations continue to assume a fully saturated troposphere and to omit cloud feedback (*Kitzmann et al., 2010; Zsom et al., 2012*). *Abe et al. (2011)* and *Leconte et al. (2013)* performed 3D modeling of rocky planets and show that the inner boundary of the HZ strongly depends on the water reservoir of the planet itself. Water ice may form at the polar caps or on the night side of a tidally locked planet, allowing for liquid water at some transitional regions. *Von Paris et al. (2010)* and *Wordsworth et al. (2010)* presented the first (1D) studies to simulate the climate of Gl 581d, which lies close to the outer edge of the HZ, finding that the planet could be potentially habitable assuming several bars of a CO₂-atmosphere. *Wordsworth et al. (2011)* studied Gl 581d with a 3D climate model, also showing that not only the amount atmospheric CO₂ determines its habitability but also the water reservoir and the resonance between the orbital and rotational period of the planet.

The fact that a planet lies within the HZ of its parent star does not guarantee that it will be habitable. Life depends on other elements besides C, O, and H and on other compounds besides water. In particular, the elements N, P, and S all play critical roles in terrestrial life. N is a constituent of both the amino acids in proteins and the nucleic acids in RNA and DNA. P is needed for the phosphate linkages between nucleotides in the latter two compounds, and S is needed for some particular amino acids. The compounds formed by these elements are termed volatiles because they are typically gases or liquids at room temperature. Habitable planets therefore require sources of volatiles. Earth's volatiles are mostly thought to have originated from the asteroid belt or beyond (*Morbidelli et al., 2000; Raymond et al., 2004*); hence, modes of planetary accretion must be considered. To hold onto its water, a planet needs an atmosphere in addition to H₂O vapor. Planets that are too small, like Mars, are thought to lose their atmospheres by various thermal and non-thermal processes, as discussed later in this chapter. Planetary magnetic fields may also be im-

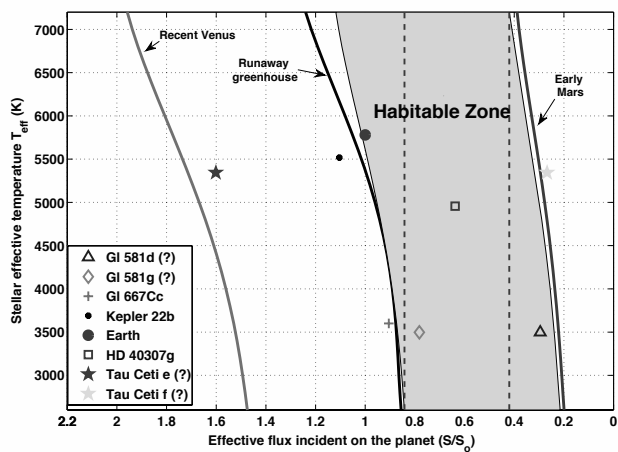


Fig. 1.— Habitable-zone boundaries in incident flux as a function of stellar T_{eff} . The gray area is delineated by the (conservative) moist greenhouse (inner border) and the maximum greenhouse (outer border). Somewhat wider HZ are possible, especially related to empirical findings on early Mars and recent Venus. The loci of various exoplanets and the Earth are marked. (From *Kopparapu et al.*, 2013; © AAS. Reproduced with permission.)

portant. Mars, which lacks an intrinsic magnetic field, has had much of its atmosphere stripped by direct interaction with the solar wind. Venus, on the other hand, also lacks an intrinsic magnetic field; yet it has successfully held onto its dense CO_2 atmosphere, suggesting that planetary size is important. Atmospheric composition may also be important, as a less CO_2 -rich atmosphere on Venus would have been hotter and more extended in its upper parts and may not have been as well retained. In the following sections of this chapter, we discuss in more detail various factors that contribute to planetary habitability. We focus on *astrophysical* conditions, while geophysical factors (such as internal heat sources, plate tectonics, land mass fraction, outgassing, volcanism or magnetic dynamos), lower-atmosphere issues (climate, winds, clouds), or biological conditions (damaging radiation doses, extreme biological environments) are not considered here.

3. DYNAMICS AND WATER TRANSPORT

3.1 Dynamics and Stability

The evolution of a biosphere is a very gradual process occurring over long time intervals. The long-term stability of a terrestrial planet moving in the HZ is therefore certainly one of the basic requirements for the formation of life on such a planet. The eccentricity of a planetary orbit is a crucial factor in orbital dynamics because only a sufficiently small value guarantees that the planet remains within the HZ. However, to assure appropriate conditions for habitability, the dynamics of the whole planetary system matter. For extensive reviews, we refer the reader to the chapters

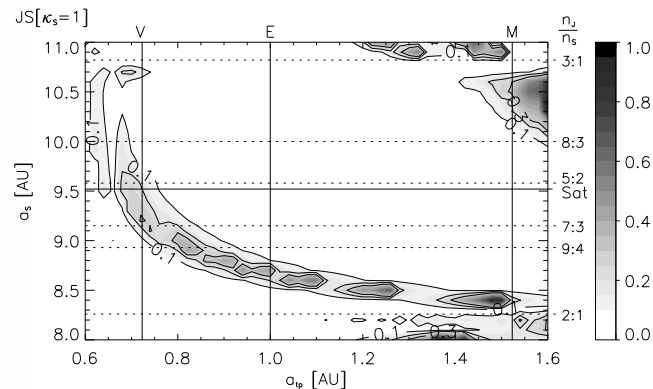


Fig. 2.— Maximum-eccentricity map for test planets under the influence of Jupiter and Saturn. The x axis shows the initial semi-major axis of the test planet and the y axis indicates the variation of the semi-major axis of Saturn. Vertical solid lines indicate the positions of Venus (V), Earth (E) and Mars (M) and the horizontal solid line shows the actual position of Saturn (Sat). The dashed horizontal lines represent the mean motion resonances (MMRs) of Jupiter and Saturn. The grey scale indicates maximum eccentricities of the test planets. (From *Pilat-Lohinger et al.*, 2008; © AAS. Reproduced with permission.)

by *Raymond et al.*, *Baruteau et al.*, *Benz et al.*, and *Davies et al.* in this volume. We focus on selected issues directly relevant for habitable-zone planets here.

Observations of planetary systems and numerical studies indicate that planets are not born where we find them today. Simulations of the late stage of formation of the outer solar system show that the giant planets arrived at their current configuration through a phase of orbital instability. The so-called *Nice Models* (e.g., *Tsiganis et al.*, 2005, *Morbidelli et al.*, 2007) provide the best-matching results for the final configuration of the outer solar system. These simulations start with a more compact system of the four giant planets (in a multi-resonant configuration in the latest version); it then experiences slight changes in the orbits due to planetesimal-driven migration leading to a resonance crossing of Saturn. This crossing causes an unstable phase for the giant planets with faster migration toward the final orbits. While during planetesimal-driven migration dynamical friction dampens orbit eccentricities, the resonance crossing will increase eccentricities and the orbits will diverge from each other (*Chiang*, 2003; *Tsiganis et al.*, 2005).

Since Jupiter and Saturn exert a strong influence on the inner solar system through secular perturbations, a change of the orbital separation of the two giant planets will modify the secular frequencies of their orbits. For example, *Pilat-Lohinger et al.* (2008) studied the secular influence of Jupiter and Saturn on the planetary motion in the HZ of a G2V star for various separations of the two giants. While Jupiter was fixed at its actual orbit 5.2 AU, Saturn's initial semi-major axis was varied between 8.0 and 11.0 AU.

Fig. 2 gives a global view of the perturbations of vari-

ous Jupiter-Saturn configurations on the HZ of a Sun-type star. We can clearly see that most of the area in the a_{TP} - a_s plot (semi-major axes for the terrestrial planet and Saturn, respectively) is not perturbed by the two giant planets, but note the arched band showing higher maximum eccentricities for test planets. This is due to the secular frequency associated with the precession of the perihelion of Jupiter. Special attention should be paid to the location of Earth's orbit, where strong variations of the eccentricity (up to ≈ 0.6) can be observed for semi-major axes of Saturn between 8.5 and 8.8 AU. We thus see that the dynamical evolution of giant planets is of utmost relevance for habitability conditions on Earth-like planets.

The huge diversity of planetary systems differing significantly from the architecture of our solar system suggests very different evolutionary tracks where processes like planet migration, planet-planet scattering, resonant trapping, mutual collisions or hyperbolic ejections influence the final constitution of a planetary system. Observations reveal large eccentricities for many exoplanets, probably indicating phases of strong interactions.

Since all planets in our solar system move in nearly circular orbits, it appears that its instability phase was moderate, probably enabling the successful formation and evolution of life on Earth. It may then be questionable whether planetary systems harboring a giant planet in an eccentric orbit can provide suitable conditions for habitability at all.

On a further note, recalling that most of the stars in our galaxy are members of binary or multiple star systems, additional gravitational perturbations from the binary interactions should also be taken into account for the assessment of habitability, as shown in detail by *Eggl et al.* (2012), *Kane and Hinkel* (2013), *Kaltenegger and Haghighipour* (2013), and *Haghighipour and Kaltenegger* (2013).

3.2 Water Transport

Where did the essential water on Earth in the amount of 0.02 percent then come from? Simulations show (e.g., *O'Brien et al.*, 2006) that our terrestrial planets likely formed out of material located in a ring around their present locations, i.e., they formed in the region of the habitable zone. However, both meteoritic evidence as well as evolutionary disk models show that the disk in this region was too warm to allow for the presence of sufficient amounts of water in solids. Therefore, water (ice) delivery should have happened later; the sources were unlikely to be comets, because statistically their collision probability with the Earth is too low (*Morbidelli*, 2013). Current thinking is that the chondritic material from the outer asteroid belt is primarily responsible for the Earth's water content. Water from chondritic asteroid material also - in contrast to many comets - on average matches the Earth ocean water D/H ratio. For a summary on these aspects, we also refer to the chapter by *van Dishoeck et al.* in this volume.

The growth of the planetesimals to protoplanets and finally planets is closely connected with the collisions of the

bodies in the early evolution of a planetary system. Such collisions may lead to the enrichment of water, depending on the origin of the colliding bodies. Various simulations (e.g., *Raymond et al.*, 2004, 2009; *O'Brien et al.*, 2006; see chapter by *Raymond et al.* in this volume) produce solar systems akin to ours, but aiming at reproducing properties of our own solar system in detail has repeatedly led to results contradicting one or several properties (masses of inner planets, eccentricities, water content of inner planets, asteroid belt architecture; *Raymond et al.*, 2009). The simulations, however, very sensitively depend on the initial conditions and the distribution of the planetesimals. Growth of terrestrial planets via collisions (with bodies from the dry inner regions, and also the water-rich outer regions of the asteroid belt) is often thought to take place when the disk gas has disappeared and only massive solid bodies remain. The mutual perturbations between these planetary embryos lead to orbital crossings and collisions; additionally, giant planets such as Jupiter trigger collisions.

The general assumption now is that about 10% of the mass of the Earth accreted from beyond 2.5 AU, suggesting that the composition of the relevant planetary embryos is close to the composition of carbonaceous chondrites which contain of order 5–10% of water (e.g., *Lunine et al.*, 2011).

Walsh et al. (2011) developed a new model that seems to explain several solar-system features: A planetesimal disk still embedded in gas is present inside 3 AU (i.e., volatile-poor S-types) as well as between and outside the gas giants (water-rich C-types). Jupiter migrated inward when Saturn was still accumulating mass; Saturn also started to migrate inward because of scattering of rocky planetesimals out from the inner part of the belt. The two planets eventually fell into the 2:3 mean motion resonance, with Jupiter located at 1.5 AU; meanwhile, the giants had scattered S-type planetesimals outward and confined the inner planetesimal disk to about 1-1.5 AU. Now, at resonance, the inward migration stopped and both giants started to migrate outwards again, up to the moment when the disk gas had dissipated. During the outward motion, Jupiter and Saturn scattered predominantly dry respectively wet planetesimals back into the inner solar system, forming the asteroid belt with its characteristic gradient of volatiles. Further scattering and collision of the forming terrestrial planets with the water-rich planetesimals eventually accumulated water on the inner planets. This “Grand Tack” scenario is depicted in Fig. 3 (sketch after the original articles by *Walsh et al.*, 2011 and *Morbidelli*, 2013). Its end point could be the starting point for the “Nice Model” mentioned in Sect. 3.1, organizing the architecture of the present-day outer solar system and finally inducing the Late Heavy Bombardment after some 800 Myrs. The “Grand Tack” model successfully explains several features relevant for habitability of the inner solar-system planets (eccentricities, planetary masses, water content).

It is important that the collisions building up the water content on Earth occurred with velocities smaller than the escape velocity from the planetesimals or protoplanets, in

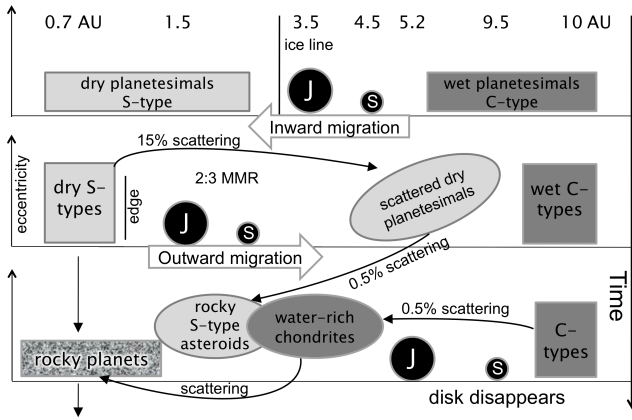


Fig. 3.— Schematic view of the formation of planets in the habitable zone of the solar system according to the “Grand Tack” model (after Walsh *et al.*, 2011; Morbidelli, 2013).

order to ensure that complete merging of the bodies occurs (Stewart and Leinhardt, 2012; Dvorak *et al.*, 2012, Maindl & Dvorak, 2014; Maindl *et al.*, 2013).

Obviously, the scenario for the water delivery to Earth is still incomplete and depends highly on the initial conditions one is using.

4. THE HOST STAR IN TIME

The conditions on the surface and in the atmospheres of terrestrial planets are controlled by the radiative and particle output of the host star; as this output varies on time scales of minutes to billions of years, conditions in planetary atmospheres are temporarily or permanently modified.

The photospheric radiative output is a consequence of the nuclear energy production in the star’s interior; it dominates the optical and partly the near-ultraviolet (NUV) spectrum. The star’s effective temperature and its luminosity follow from the laws of stellar structure and consequent nuclear reactions in the core, which gradually vary in time.

In contrast, radiation in the ultraviolet (UV, 2100–3500 Å), the far-ultraviolet (FUV, 912–2100 Å), the extreme ultraviolet (EUV, 100–912 Å), and the X-ray (< 100 Å) range is a consequence of (often violent) energy release in the stellar atmosphere due to annihilation of unstable magnetic fields. Magnetic activity is expressed in cool photospheric spots, chromospheric plage emitting in the ultraviolet, and hot (million-degree) coronal plasma in “magnetic loops” with strong X-ray radiation; also, highly-energetic, accelerated particles, shock fronts from mass ejections, short-term energetic flares and perhaps also the solar wind indicate the operation of magnetic energy release. Magnetic fields are ultimately generated in a magnetic dynamo in the stellar interior, driven by the interaction between convection and differential rotation. The short-wavelength stellar output is therefore a function of stellar rotation (depending on stellar age) and of the stellar spectral type (determining the depth of the convection zone, itself

also somewhat dependent on age).

A late-type star’s rotation period, P , steadily declines during its main-sequence life (see chapter by *Bouvier et al.* in this volume). This is consequence of the stellar magnetic field permeating the ionized stellar wind which transports away angular momentum. The declining rotation period itself feeds back to the dynamo, weakening the production of magnetic activity. As a consequence, P not only declines in time but it converges, after a few hundred million years for a solar analog, to a value dependent on age but independent on the initial Zero-Age Main Sequence (ZAMS) rotation rate. Magnetic activity and the related XUV (FUV, EUV, and X-ray) output therefore also become a function of stellar age. A generalized formula has been derived by *Mamajek and Hillenbrand* (2008) namely $P = 0.407([B-V]_0 - 0.495)^{0.325} t_6^{0.566}$ [d] where $[B-V]_0$ is the intrinsic stellar $B - V$ color and t_6 is the stellar age in Myr. For younger stars, the rotation period also depends on the presence of a circumstellar disk (around pre-main sequence stars) leading to “disk-locked”, relatively slow rotation, and the history of disk dispersal before the arrival on the main sequence (MS), leading to a wide range of ZAMS rotation periods (*Soderblom et al.*, 1993).

4.1 The Evolution of Stellar Optical Radiation

Before arriving on the MS, a star’s luminosity first decreases when it moves down the Hayashi track as a T Tauri star; in that phase, the Sun was several times brighter than today, although its effective temperature was lower ($T \approx 4500$ K) and its radius consequently larger ($\approx 2 - 3R_\odot$). Before reaching the ZAMS, solar-like stars reach a minimum bolometric luminosity, L_{bol} , which for a solar-mass star is as low as $\approx 0.45L_{\text{bol},\odot}$ (at an age of ≈ 13 Myr; *Baraffe et al.*, 1998).

The Sun’s bolometric luminosity has steadily increased since its arrival on the ZAMS, starting from $\approx 70\%$ of today’s luminosity. At the same time, the effective temperature also increased somewhat (*Sackmann & Boothroyd*, 2003). This increase is a consequence of the evolution of nuclear reactions in the core of the star. Similar trends hold for other cool main-sequence stars.

During the later MS evolution, the Sun’s brightness will increase up to $\approx 3L_\odot$ at an age of 10 Gyr. The significant change in L_{bol} implies that the classical habitable zone around the star moves outward during this evolution. *Kasting et al.* (1993) derived the HZ-width for the entire main-sequence evolution of the Sun (and cooler stars), defining the “continuously habitable zone”. The latter becomes narrower as the inner border moves outward while - under the assumption that planets moving into the HZ at a later time do not evolve into habitable planets - the outer border remains the same. Therefore, the total width of the HZ narrows as the star evolves. The Earth will in fact be inside the inner HZ radius at an age of ≈ 7 Gyr, i.e., only 2.4 Gyr in the future (for the most pessimistic models) and so it will lose its water. This effect is less serious for later-type stars

for the same time interval because of their slower evolution.

4.2 Evolution of Stellar Ultraviolet Radiation

The stellar FUV-NUV flux ($91.2 \leq \lambda \leq 350$ nm) covers the transition from the emission spectrum of the hot chromospheric/transition region gas, at typical temperatures of $10^4 - 10^5$ K, to the rising photospheric emission, dominating above ~ 200 nm. This wavelength range contains the strongest emission line, H Ly α , which is responsible for over 50% of the stellar high-energy (XUV) flux. The UV domain is especially relevant in the context of planetary atmospheres since UV photons trigger a variety of photochemical reactions (e.g., *Hu et al.*, 2012; *Yung and DeMore*, 1999; Sect. 5.1 below). Important molecules such as H₂O, CO₂, CH₄, CO, NH₃, have photodissociation cross sections that become significant below 200 nm. Also, the abundance of the biosignature molecule O₃ is mainly controlled by photochemical reactions, hence understanding the interaction of the stellar radiation with the atmospheric chemistry is of great importance for the determination of possible atmospheric biosignatures. A reliable calculation of the photodissociation rates and their time evolution is very complex due to the interplay between the strongly decreasing cross sections and the rapidly rising stellar flux toward longer wavelengths. For example, the flux of solar-like stars increases by more than 2 orders of magnitude from 150 to 200 nm and the photodissociation cross section of, e.g., H₂O, decreases by over 3 orders of magnitude in the same interval.

The FUV-NUV flux from low-mass stars is variable over many time scales, including hours (flares), days (rotation period), years (activity cycles) and Gyr (rotational spin-down). We focus here on the long-term evolution, which is comparable to the nuclear time scale. The UV photospheric flux (i.e., $\lambda \gtrsim 200$ nm) rises with time as the star evolves off the ZAMS and increases its radius and effective temperature. For the case of the Sun, the overall Main Sequence UV flux increase ranges within 30%–200% depending on the wavelength, as illustrated by *Claire et al.* (2012) on the basis of Kurucz atmosphere models.

The chromospheric and transition region emission is much more difficult to describe, as it depends on the evolution of the magnetic properties of the star. A successful technique employed to investigate the long-term evolution of stellar activity is to identify stars that can act as proxies for different ages (e.g., *Ribas et al.*, 2005). In the UV this is especially complicated by the difficulty in finding stars that are close enough to an evolutionary track and by the need to use space facilities (FUSE, GALEX, IUE, HST) that have only been able to provide high-quality data for a limited number of nearby objects. The best example of the application of the proxy technique is the star κ^1 Cet, which is a close match to the Sun at an age of ~ 0.6 Gyr, as presented by *Ribas et al.* (2010). *Claire et al.* (2012) generalized the study to the entire main sequence evolution of solar-like stars, resulting in approximate flux multipliers as a function

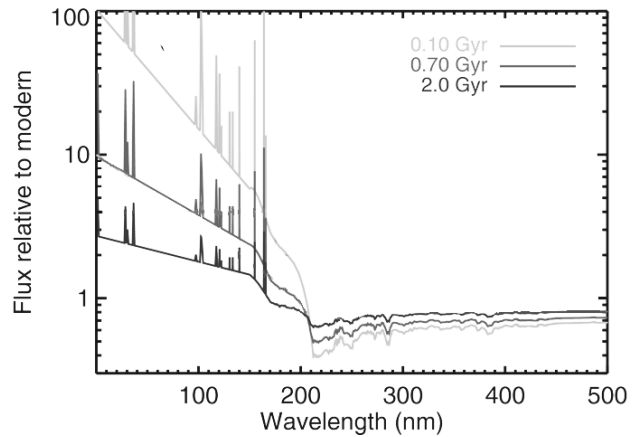


Fig. 4.— Flux ratios relative to the modern (present-day) Sun at 1 AU covering the UV range of solar-like stars of different ages. Both continuum and line fluxes are included using the procedure in *Claire et al.* (2012). (Adapted from *Claire et al.* 2012; © AAS. Reproduced with permission.)

of wavelength that can be applied to the current solar flux to calculate the spectral irradiance at different ages. Figure 4 plots the flux multipliers. Better constraints to the UV flux evolution of solar-like stars will follow from observations with new instrumentation (*Linsky et al.*, 2012).

The flux multipliers of *Claire et al.* (2012) are appropriate for the Sun and solar-like stars but may not be adequate for stars of lower mass. Measurements of UV fluxes of a handful of M dwarfs are available (*France et al.*, 2013, and references therein). *France et al.* (2013) show that the flux in the FUV band relative to the NUV band for most M dwarfs is 3 orders of magnitude larger than the solar value, and this has strong photochemical implications. But, in spite of these measurements, we still lack information on the time evolution of such fluxes, the main reason being the difficulty in estimating stellar ages. The development of new alternative age determination methods for MS K and M dwarfs (*Garcés et al.*, 2011) should help to define the necessary UV flux-time relationships.

The determination of the H Ly α line flux deserves special attention. Precise measurement of the H Ly α line is extremely challenging due to contamination from Earth geocoronal emission and the difficulty of correcting interstellar and astrospheric absorption (*Wood et al.*, 2005). *Linsky et al.* (2013) present a compilation of HST/STIS observations of a relatively large sample of stars from F to M spectral types, with Ly α fluxes and correlations with other emission line fluxes. When normalizing fluxes to the stellar habitable zone, *Linsky et al.* show a clear increasing trend of Ly α flux with decreasing stellar T_{eff} . M dwarfs produce, on average, a nearly one order of magnitude higher Ly α flux in their HZ than do solar-like stars in their respective HZ. Unfortunately, most of the stars used by *Linsky et al.* have no well-determined ages and thus a time-evolution determination is not possible. The Ly α flux evolution relationship of

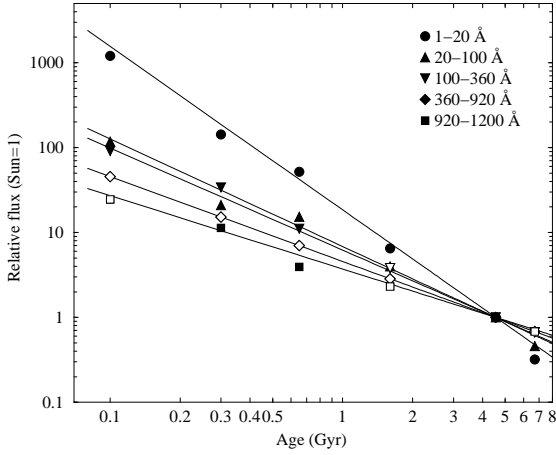


Fig. 5.— Power-law decay of spectral output of a solar analog during its MS (age 0.05–10 Gyr) life, normalized to the present-day solar flux. The shortest-wavelength flux decays the fastest. (From *Ribas et al.*, 2005; © AAS. Reproduced with permission.)

Ribas et al. (2005) for solar analogs is still up to date:

$$F \approx 19.2t_9^{-0.72} \text{ [erg s}^{-1} \text{ cm}^{-2}] \quad (1)$$

where F is the normalized flux at a distance of 1 AU and t_9 is the stellar age in Gyr.

4.3 Evolution of High-Energy Radiation and Activity

The strongest evolutionary change in magnetically induced stellar radiation is seen in the high-energy range including EUV, X-ray and gamma-ray radiation. The integrated luminosity in the soft X-ray (0.1–10 keV photon energy) and the EUV (0.014–0.1 keV) depends on the stellar rotation period, P , and therefore age; for a solar analog (*Güdel et al.*, 1997; *Sanz-Forcada et al.*, 2011),

$$L_X \approx 10^{31.05 \pm 0.12} P^{-2.64 \pm 0.12} \text{ [erg s}^{-1}] \quad (2)$$

$$L_X \approx (3 \pm 1) \times 10^{28} t_9^{-1.5 \pm 0.3} \text{ [erg s}^{-1}] \quad (3)$$

$$L_{\text{EUV}} \approx (1.3 \pm 0.3) \times 10^{29} t_9^{-1.24 \pm 0.15} \text{ [erg s}^{-1}] \quad (4)$$

(t_9 is the stellar age in Gyr). However, these dependencies only hold for sufficiently slow rotation. For young, rapid rotators, magnetic activity and therefore the X-ray output reaches a saturation level. Empirically, $L_X \approx 10^{-3} L_{\text{bol}}$ for all late-type main-sequence and pre-main sequence stars.

These dependencies can be generalized to stars of other spectral class. For example, using the Rossby number $Ro = P/\tau_c$ (where τ_c is the spectral-class and age-dependent convective turnover time), one finds a unified description of the $L_X - Ro$ and $L_X - P$ dependencies (*Pizzolato et al.*, 2003), namely $L_X \approx 10^{-3} L_{\text{bol}}$ for rapid rotators (young age) and $L_X \propto P^{-2}$ for slow rotators (more evolved stars).

Combining these trends with the mass or spectral-type dependent spin-down rate of a star has important consequences for the stellar high-energy output in time. Attempts to unify the X-ray decay law were described in *Scalo et al.*

(2007), *Guinan et al.* (2009) and *Mamajek & Hillenbrand* (2008). M dwarfs, for example, remain at the saturation level for much longer than solar-like stars, up to order of a Gyr as for example seen in the Hyades cluster (*Stern et al.*, 1995), in contrast to a solar analog that leaves this regime typically in the first 100 Myr.

A second evolutionary trend in X-rays is due to the average coronal temperature, resulting in a long-term trend in spectral hardness. X-ray hardness is an important factor determining the penetration depth of X-rays into a planetary atmosphere. While the present-day solar corona shows an average temperature, T_{cor} , of about 2 MK, young, magnetically active stars reveal T_{cor} around 10 MK and even higher, implying a corresponding shift of the dominant spectral radiation to harder photon energies (≈ 1 keV). The empirical relation for solar-mass stars is (*Telleschi et al.*, 2005)

$$L_X = 1.61 \times 10^{26} T_{\text{cor}}^{4.05 \pm 0.25} \text{ [erg s}^{-1}]. \quad (5)$$

This relation holds similarly for pre-main sequence stars.

Short-wavelength (UV to X-ray) emission-line fluxes $F(T_{\text{max}}, t)$ for maximum line formation temperatures T_{max} ($4 \lesssim \log T_{\text{max}} \lesssim 7$) decay in time (t_9 in Gyr) as

$$F(T_{\text{max}}, t) = \alpha t_9^{-\beta} \quad (6)$$

$$\beta = 0.32 \log T_{\text{max}} - 0.46 \quad (7)$$

(*Güdel*, 2007; similar relations hold for the continuum, where T_{max} corresponds to $hc/(\lambda k)$, h is the Planck constant, k the Boltzmann constant, c the speed of light, and λ the continuum wavelength). In other words, the decay is *steeper for shorter wavelengths*, implying the largest enhancement factors for young stars for the shortest wavelengths (Fig. 5). The average enhancement factors are summarized in Table 1 for a solar analog throughout its main-sequence life. We emphasize that enhancement factors for individual young stars may scatter around the given values because the rotation period may not have converged to an age-independent value on the main sequence. We refer to the chapter of *Bouvier et al.* in this volume for more details on the rotational evolution of stars.

4.4 The Evolution of Stellar Winds and Mass Loss

In addition to being exposed to electromagnetic radiation from their host stars, planets are also exposed to high-speed outflows of particles from the stellar atmosphere. For cool main sequence stars like the Sun, stellar winds arise in the hot coronae that represent the outermost atmospheres of the stars. Although the mechanisms of coronal heating and coronal wind acceleration remain hot topics of research, *Parker* (1958) demonstrated long ago that once you have a hot corona, a wind much like that of the Sun arises naturally through thermal expansion. Thus, any star known to have a hot corona can be expected to possess a coronal wind something like that of the Sun. Observations from X-ray observatories such as *Einstein*, *ROSAT*, *Chandra*, and

TABLE 1
 ENHANCEMENT FACTORS OF X-RAY/EUV/XUV/FUV FLUXES IN SOLAR HISTORY^a

Solar age (Gyr)	Time before present (Gyr)	Enhancement in		
		X-Rays (1–20 Å)	Soft-X (20–100 Å) EUV (100–360 Å)	FUV (920–1180 Å)
0.1	4.5	1600 ^b	100	25
0.2	4.4	400	50	14
0.7	3.9	40	10	5
1.1	3.5	15	6	3
1.9	2.7	5	3	2
2.6	2.0	3	2	1.6
3.2	1.4	2	1.5	1.4
4.6	0	1	1	1

^a normalized to ZAMS age of 4.6 Gyr before present

^b large scatter possible due to unknown initial rotation period of Sun

XMM-Newton have demonstrated that X-ray emitting coronae are ubiquitous among cool main sequence stars, so coronal winds can be expected to be ubiquitous as well.

Unfortunately, detecting and studying these winds is much harder than detecting and studying the coronae in which they arise. Current observational capabilities do not yet allow us to directly detect solar-like coronal winds emanating from other stars. Bremsstrahlung radio emission may uncover ionized winds. An upper limit for the mass-loss rate of $\dot{M}_w \lesssim 2 \times 10^{-11} M_\odot \text{ yr}^{-1}$ was inferred for the F5 IV-V subgiant Procyon (*Drake et al.*, 1993), and $\dot{M}_w \lesssim 7 \times 10^{-12} M_\odot \text{ yr}^{-1}$ for the M dwarf Proxima Centauri (using a wind temperature $T_w = 10^4$ K and a wind velocity $v_w = 300 \text{ km s}^{-1}$, *Lim et al.*, 1996). *Van den Oord and Doyle* (1997) also found $\dot{M}_w \lesssim 10^{-12} M_\odot \text{ yr}^{-1}$ for observed dMe stars assuming $T_w \approx 1$ MK. For young (few 100 Myr) solar analogs, *Gaidos et al.* (2000) found upper limits of $\dot{M}_w \lesssim (4-5) \times 10^{-11} M_\odot \text{ yr}^{-1}$.

Sensitive upper limits can also be derived from the absence of radio attenuation of coronal (flare or quiescent) radio emission by an overlying wind (*Lim and White*, 1996). This method applies only to spherically symmetric winds. The most sensitive upper limits based on low-frequency radio emission apply to the dMe star YZ CMi, with $\dot{M}_w \lesssim 5 \times 10^{-14} M_\odot \text{ yr}^{-1}$, $\lesssim 10^{-12} M_\odot \text{ yr}^{-1}$, and $\lesssim 10^{-11} M_\odot \text{ yr}^{-1}$ for $v_w = 300 \text{ km s}^{-1}$ and $T_w = 10^4$ K, 10^6 K, and 10^7 K, respectively.

Alternatively, neutrals of the interstellar medium flowing into an astrosphere blown by a stellar wind may induce charge exchange that could in principle be detected by the ensuing line emission at X-ray wavelengths. Spatially resolved observations are needed, but again, no detection has been reported yet (see *Wargelin and Drake*, 2001).

The so far only successful method relies not on detecting the winds themselves, but their collision with the ISM (*Linsky and Wood*, 1996). The collision regions are called “astrospheres,” analogous to the “heliosphere” that defines the solar wind’s realm of influence around the Sun. Because

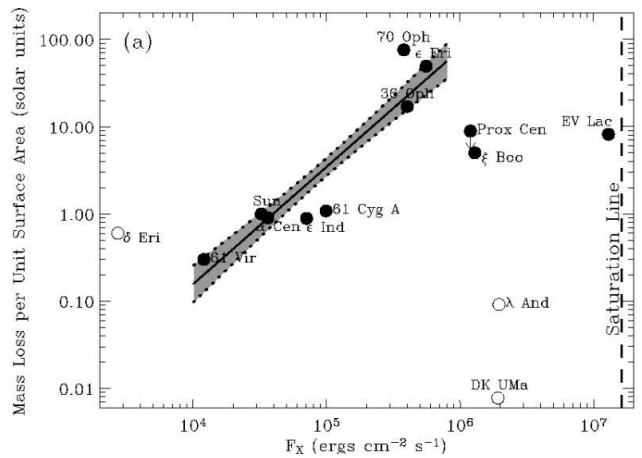


Fig. 6.— Mass-loss rates per unit surface area vs. stellar X-ray surface fluxes. MS stars are shown by filled circles. (From *Wood et al.*, 2005; © AAS. Reproduced with permission.)

the ISM surrounding the Sun is partially neutral, the solar-wind/ISM collision yields populations of hot hydrogen gas throughout the heliosphere created by charge exchange processes. The highest H I densities are in the so-called “hydrogen wall” just beyond the heliopause, hundreds of AU from the Sun. Ultraviolet spectra from the *Hubble Space Telescope* (HST) have detected Lyman- α absorption from both the heliospheric hydrogen wall (*Linsky and Wood*, 1996), and astrospheric hydrogen walls surrounding the observed stars (*Gayley et al.*, 1997; *Wood et al.*, 2002, 2005). In the case of astrospheres, the amount of absorption is related to the strength of the stellar winds, so with guidance from hydrodynamic models of the astrospheres, stellar mass loss rates have been inferred from the astrospheric Lyman- α data. The number of astrospheric wind measurements is only 13, however, and many more measurements are required for further progress to be made in this area.

These observations imply that winds generally correlate with stellar activity (*Wood et al.*, 2005; Fig. 6). The mass-

loss rate \dot{M}_w per unit stellar surface correlates with the stellar X-ray surface flux F_X ; correspondingly, the total mass-loss rate \dot{M}_w correlates with the X-ray luminosity L_X and therefore age, t ,

$$\dot{M}_w \propto L_X^{1.34 \pm 0.18} \quad (8)$$

$$\dot{M}_w \propto t^{-2.33 \pm 0.55} \quad (9)$$

where for the second formula the activity-age relation has been used (Wood *et al.*, 2005). Extrapolating the above law up to the X-ray saturation limit at $F_X \approx 2 \times 10^7 \text{ erg cm}^{-2} \text{ s}^{-1}$, we would infer \dot{M}_w of the youngest solar analogs to exceed the present-day solar mass loss ($\dot{M}_\odot \approx 2 \times 10^{-14} M_\odot \text{ yr}^{-1}$; e.g., Feldman *et al.*, 1977) by a factor of a thousand. However, there is some evidence that the most active stars with $F_X \gtrsim 8 \times 10^5 \text{ erg cm}^{-2} \text{ s}^{-1}$ are inconsistent with this correlation and may actually have surprisingly weak winds (Wood *et al.*, 2005). Mass loss appears to increase with activity up to about $\dot{M}_w = 100$ times the current solar wind, but then appears to actually weaken towards even higher stellar activity, down to about 10 times the current solar mass loss rate. Possibly, the appearance of high-latitude active regions (spots) with a magnetic field more akin to a global dipole may inhibit wind escape (Wood *et al.*, 2005).

We emphasize that this method requires the presence of *neutrals* (e.g., at least a partially neutral cloud) around the observed star. If the interstellar medium around the star is fully ionized, no hydrogen walls can form, and the absence of absorption features in Ly α will *not* indicate weak winds.

4.5 Stellar Flares

A stellar flare is the result of short-term (minutes to hours) explosive energy release tapped from non-potential energy in the coronal magnetic fields, ultimately derived from convective energy at the stellar surface. During flares, plasma in the stellar atmosphere is rapidly heated, and therefore fluxes increase across the electromagnetic spectrum, in very rare cases exceeding the entire quiescent stellar output (Osten *et al.*, 2010). Flare radiation amplitudes are particularly high in the short-wavelength (XUV, gamma-ray) range, and also in the radio regime.

Flares occur at rates depending on the flare amplitude or its released (radiative or total) energy, E , in the form of a power law, $dN/dE \propto E^{-\alpha}$, where $\alpha \approx 2 \pm 0.4$ has been found by various investigators, i.e., small flares occur at a much higher rate than the rare big flares (Güdel, 2004, and references therein).

Very energetic flares or “superflares” may contribute to the ionization of upper planetary atmospheres (ionospheres) and upper-atmospheric chemistry, thus potentially changing planetary habitable conditions. Audard *et al.* (2000) found that the rate of large EUV flares exceeding some given radiative energy threshold is proportional to the average, long-term X-ray luminosity of the star, suggesting a very high rate of superflares in young, active stars. This relation

at the same time indicates that superflares are not occurring at a higher rate in M dwarfs than in solar analogs; it is the closer-in habitable zones around M dwarfs combined with the slower decay of M-dwarf activity that subjects habitable planets around M dwarfs to much higher flare-radiation doses for a longer time.

Schrijver *et al.* (2012) investigated the presence of superflares on the Sun in historical times, using natural archives (nitrate in polar ice cores and various cosmogenic radionuclids) together with flare statistics and the historical record of sunspots; they conclude that flares in the past four centuries are unlikely to have exceeded the largest observed solar flare with total energy of $\approx 10^{33} \text{ erg}$. The solar magnetic field (an similarly, stellar magnetic fields) provides an upper bound to the maximum flare energy release simply by the amount of free magnetic energy that could coherently be converted. This limit is indeed about $\approx 10^{33} \text{ erg}$, a tenfold stronger flare requiring a spot coverage of 10%, unobserved on the modern Sun (Schrijver *et al.*, 2012).

However, Schaefer *et al.* (2000) reported, from observations in various wavebands, nine “super-flares” with total radiative energies of $10^{33} - 10^{38} \text{ erg}$ on solar (F-G type) analog stars, none of which is exceptionally young or extremely active, or a member of a close binary system. Some of the flaring objects were even older than the Sun. They concluded that the average recurrence time for superflares on such stars may be decades to centuries although this would obviously be an overestimate for the Sun. With the new Kepler satellite data in hand, Maehara *et al.* (2012) found surprisingly many superflares with bolometric energies of $10^{33} - 10^{36} \text{ erg}$, with an estimated recurrence time of $\approx 800 \text{ yrs}$ for 10^{34} erg flares on old, solar-like stars. None of these stars is known to host close-in exoplanets that could induce such energy release.

The impact of stellar flares on the atmospheres of terrestrial extrasolar planets has been studied by, e.g., Segura *et al.* (2010) and Grenfell *et al.* (2012). The importance of such single events would be their potential to melt ice surfaces on habitable planets, the possible temporary breakup of the ionosphere and ozone depletion after creation of nitrogen oxides in the irradiated atmosphere; an event of 10^{36} erg (ionizing energy) was estimated to result in a loss of 80% of the total ozone content for more than one year, with the consequent increase in UV irradiation (Schaefer *et al.*, 2000).

4.6 Coronal Mass Ejections

Apart from stellar winds, exoplanets may interact with coronal mass ejections (CMEs), occurring sporadically and propagating within the stellar wind as large-scale plasma-magnetic structures. The high speeds of CMEs (up to thousands of km/s), their intrinsic magnetic field and their increased density compared to the stellar wind background make CMEs an active factor which strongly influences the planetary environments and magnetospheres. Often, collisions of the close-orbit exoplanets with massive stellar

CME plasmas compress planetary magnetospheres much deeper towards the surface of the exoplanet. This would result in much higher ion loss rates than expected during the usual stellar wind conditions (see Sect. 6 below).

CMEs can be directly observed only on the Sun. They are associated with flares and prominence eruptions and their sources are usually located in active regions and prominence sites. The likelihood of CME events increases with the size and power of the related flare event. Generally, it is expected that the frequent and powerful flares on magnetically active flaring stars should be accompanied by an increased rate of CME production. Based on estimates of solar CME plasma density n_{CME} , using the in-situ spacecraft measurements (at distances > 0.4 AU) and the analysis of white-light coronagraph images (at distances $\leq 30R_{\text{Sun}} \approx 0.14$ AU), *Khodachenko et al.* (2007a) provided general power-law interpolations for the n_{CME} dependence on the orbital distance d (in AU) to a star:

$$n_{\text{CME}}^{\min}(d) = 4.88d^{-2.3}, \quad n_{\text{CME}}^{\max}(d) = 7.10d^{-3.0}. \quad (10)$$

Equations (10) identify a typical maximum-minimum range of n_{CME} . The dependence of stellar CME speed v_{CME} on d can be approximated by the formula:

$$v_{\text{CME}} = v_0 \left(1 - \exp \left[\frac{2.8R_{\text{Sun}} - d}{8.1R_{\text{Sun}}} \right] \right)^{1/2}, \quad (11)$$

proposed in *Sheeley et al.* (1997) on the basis of tracking of several solar wind density enhancements at close distances ($d < 0.1$ AU). For the approximation of average- and high-speed CMEs one may take in Eq. (11) $v_0 = 500 \text{ km s}^{-1}$ and $v_0 = 800 \text{ km s}^{-1}$, respectively. Besides of that, the average mass of CMEs is estimated as 10^{15} g, whereas their average duration at distances of ≈ 0.05 AU is close to 8 hours.

Because of the relatively short range of propagation of most CMEs, they should strongly impact the planets in close orbits ($\lesssim 0.3$ AU). *Khodachenko et al.* (2007a) have found that for a critical CME production rate $f_{\text{CME}}^{\text{cr}} \approx 36$ CMEs per day (and higher), a close orbit exoplanet appears to be under continuous action of the stellar CMEs plasma, so that each next CME collides with the planet during the time when the previous CME is still passing over it, acting like an additional type of “wind”. Therefore, investigations of evolutionary paths of close-orbit exoplanets in potentially habitable zones around young active stars should take into account the effects of such relatively dense magnetic clouds (MCs) and CMEs, apart from the ordinary winds.

5. ATMOSPHERES AND STELLAR RADIATION

The radiation environment during the active period of a young star is of great relevance for the evolution and escape of planetary atmospheres. The visible radiation penetrates through a planetary atmosphere down to its surface unless it is blocked by clouds, aerosols or dust particles. The average skin or effective temperature, T_{eff} , of a planet can be estimated from the energy balance between the optical/near-IR

emission irradiating the planet and the mid-IR thermal radiation that is lost to space:

$$T_{\text{eff}} = \left[\frac{S(1-A)}{4\sigma} \right]^{0.25}, \quad (12)$$

with S being the solar radiative energy flux at a particular orbit location of a planet, A the bond albedo describing the fraction of the radiation reflected from the planet, and σ the Stefan-Boltzmann constant. Most of the IR radiation emitted from Venus or Earth does not come from the surface; rather, it comes from the cloud top level on Venus or the mid-troposphere on Earth and yields $T_{\text{eff}} \approx 220$ K for Venus and 255 K for Earth. Above the mesopause, radiation with short wavelengths in the X-ray, soft-X-ray and the extreme ultraviolet (XUV) part of the spectrum is absorbed in the upper atmosphere, leading to dissociation of molecular species, ionization and heating, so that the thermosphere temperature $T_{\text{th}} \gg T_{\text{eff}}$.

5.1 Surface Climate and Chemical Processing

The surface climate conditions on terrestrial planets are largely affected by the presence of greenhouse gases (main contributors: H_2O , CO_2 , O_3 , CH_4 , N_2O), absorbing and re-emitting infrared (IR) radiation and thereby heating the lower atmosphere. The greenhouse effect on the surface of Earth is about 33 K, and about 460 K for the dense CO_2 atmosphere of Venus. In the troposphere of the terrestrial planets, adiabatic cooling leads to decreasing temperatures with height. In the case of Earth, the ozone (O_3) layer peaking at about 30 km height absorbs stellar radiation around 250 nm, resulting in atmospheric heating and a stratospheric temperature inversion. This is not observed for those terrestrial planets in our solar system which do not have sufficient amounts of ozone, i.e., Mars and Venus. In the context of extrasolar planets, ozone is of special interest not only for its climatic impact, but also as a potential biosignature which can be detected by spectroscopic absorption bands in the IR spectral range.

Ozone is formed in the Earth’s stratosphere via photolytic processes from O_2 (*Chapman*, 1930) operating at wavelengths < 200 nm. The ozone molecule itself is also destroyed photolytically in the UVB and via HO_x and NO_x catalytic cycles (*Crutzen*, 1970), which are also favored by UV radiation. In the Earth’s troposphere, O_3 is mainly produced by the smog mechanism (*Haagen-Smit et al.*, 1952).

Terrestrial exoplanets orbit host stars of different types, i.e., stars with different effective temperatures and hence spectral energy distributions. Cool dwarf stars, such as M-types, exhibit less flux at optical and near-UV wavelengths than the Sun down to about 200 nm, depending on stellar class. They can, however, be very active in the UV range below 170-190 nm, hence at wavelengths relevant for photochemistry of O_2 and O_3 (Sect. 4.2). Planets with oxygen-bearing atmospheres around M dwarf stars may therefore have weaker or stronger ozone layers, depending on UV

fluxes below about 200 nm (e.g., *Segura et al.*, 2005; *Grenfell et al.*, 2013). Cool M dwarfs with reduced UV fluxes allow for less O₂ destruction and therefore less O₃ is produced by the Chapman mechanism. In the case of very cool M dwarfs this production mechanism could be severely reduced and the smog mechanism could take over even in the mid-atmosphere (*Grenfell et al.*, 2013). For Earth-like planets around such cool and quiet M dwarfs atmospheric ozone abundances can be significantly reduced, whereas the same kind of planet around an active M dwarf with high UV fluxes would show a prominent ozone layer (*Segura et al.*, 2005; *Grenfell et al.*, 2014). The amount of stratospheric ozone on exoplanets around M dwarfs may therefore highly depend on their UV activity. Surface temperatures are somewhat higher on Earth-like planets (i.e., with modern Earth type N₂-O₂ dominated atmospheres) orbiting M dwarfs for the same total stellar insolation, because, e.g., Rayleigh scattering contributes less to the planetary albedo owing to the λ^{-4} -dependence of the Rayleigh scattering coefficient. The largest impact of the different stellar energy flux distribution of cool stars on a planet's $T - p$ profile is, however, seen in the mid-atmosphere. Earth-like terrestrial exoplanets around M dwarfs do not show a strong stratospheric temperature inversion, even if a thick ozone layer is present in the mid-atmosphere (*Segura et al.* 2005; *Rauer et al.*, 2011; *Grenfell et al.*, 2013). For example, as discussed above, some active M dwarfs with very high fluxes below 200 nm can efficiently destroy oxygen to form a strong ozone layer (*Segura et al.*, 2005), but still show no stratospheric T -inversion (Fig. 7). This is primarily caused by the reduced near-UV flux of M dwarf stars around 250 nm which is relevant for stratospheric heating. In Fig. 7, increasing UV (from an inactive M7 dwarf - “ $\times 1$ ” - to $1000\times$ stronger) leads to middle atmosphere cooling because UV stimulates OH which reduces CH₄ (an important heater). On increasing UV further, however, O₃ is stimulated which leads to strong stratospheric heating. Results suggest that a strong T -inversion is less relevant for surface climate but can make the detection of atmospheric absorption bands more difficult (e.g., *Rauer et al.*, 2011; *Kaltenegger et al.*, 2011; *Grenfell et al.*, 2014). In summary, UV can, on the one hand, enhance O₃, hence heat the middle atmosphere, but on the other hand it can stimulate OH, hence remove CH₄, which has the opposite effect - which effect is strongest depends on the amount of O₃, CH₄ and the UV intensity.

Other atmospheric species relevant for climate, habitability and biosignatures, such as water, methane, or nitrous oxide are also affected by the different host star spectral energy distributions. Water and methane are strong greenhouse gases and therefore relevant for habitability. Water is produced in the stratosphere via methane oxidation ($\text{CH}_4 + 2\text{O}_2 \rightarrow \text{CO}_2 + 2\text{H}_2\text{O}$) and destroyed by photolysis. Earth-like planets around M dwarf stars show somewhat higher atmospheric water abundances for the same incident stellar flux due to higher surface temperatures and reduced stratospheric photolytic destruction. In addition,

the production of O¹D is reduced due to the reduced M dwarf UV flux, affecting the production of OH via: $\text{H}_2\text{O} + \text{O}^1\text{D} \rightarrow 2\text{OH}$. This in turn leads to reduced methane destruction, hence increased methane abundances in the atmosphere (e.g., *Segura et al.*, 2005; *Rauer et al.*, 2011). Also the good biosignature N₂O (good in the sense of attributability of spectral features to biogenic activity) could be significantly increased for planets around cool M dwarfs (*Rauer et al.*, 2011; *Seager et al.*, 2013). This is interesting because N₂O is normally not detectable for Earth-like planets around solar-like stars due to its weak spectral features, but may be detectable for planets orbiting M dwarf stars. These examples illustrate how the central star spectral energy distribution affects atmospheric chemistry, abundances and the strength of potentially observable atmospheric molecular absorption bands. The discussion has just started, and many more parameter studies are needed to identify the most dominant effects on observable signals.

Clearly, the visibility of indicators for habitability (e.g., H₂O, CO₂, CH₄) in spectra obtained from terrestrial exoplanets are significantly affected by the central star spectral type and activity (e.g., *Segura et al.*, 2005; *Selsis et al.*, 2008; *Segura et al.*, 2010; *Rauer et al.*, 2011; *Hedelt et al.*, 2013; *Grenfell et al.*, 2014; *Rugheimer et al.*, 2013). This holds in particular for M dwarfs which are favorable targets for transit spectroscopy during primary and secondary eclipse because of their improved star/planet contrast. It has become evident that a good characterization of the host star stellar energy distribution and its temporal variability is crucial for the interpretation of absorption spectra and iden-

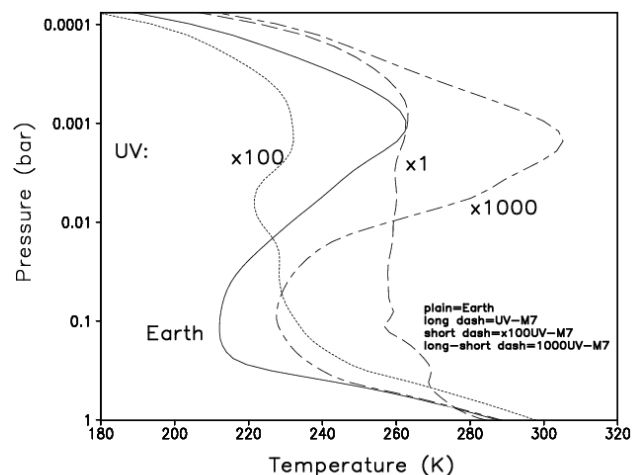


Fig. 7.— Response of the atmospheric $T - p$ profile of an Earth-like planet in the HZ of an M7 red dwarf star to UV irradiation. The profiles are for a star with very low UV flux (long dash, “ $\times 1$ ”), 100 and 1000 times this flux (dotted resp. long-short dash). The $T - p$ profile for the present Earth is also shown (solid). The cooling from $1\times$ to $100\times$ is due to the destruction of CH₄ by UV, resulting in less heating. Very high UV levels lead to a temperature inversion in the ozone layer (adapted from *Grenfell et al.*, 2014).

tification of potential false-positive signals.

Clouds are a common phenomenon in the atmospheres of many terrestrial bodies of our Solar System (e.g., Venus, Earth, Mars, Titan) and are also expected in atmospheres of terrestrial extrasolar planets. They play a major role in the climate of terrestrial planets by affecting the atmospheric energy budget in several competing ways. Clouds can scatter a fraction of the incident stellar radiation back to space, resulting in atmospheric cooling. On the other hand, by trapping thermal radiation within the lower atmosphere clouds can yield a greenhouse effect. This greenhouse effect can occur either by absorption and re-emission at their local temperature (classical greenhouse effect) or by scattering thermal radiation back toward the planetary surface (scattering greenhouse effect). In the Earth’s atmosphere, for example, low-level water clouds usually cool the surface whereas high-level water ice clouds can lead to a heating effect. The net climatic effect of a cloud is largely determined by the wavelength-dependent optical properties of the cloud particles (e.g., absorption and scattering cross-sections, single-scattering albedo, asymmetry parameter, or scattering phase function). These properties can differ considerably for different cloud-forming species, particle sizes, and shapes (see *Marley et al.*, 2013, for a broad review on clouds in the atmospheres of extrasolar planets).

The climatic effect of clouds has been discussed, for example, as possible solutions to the Faint Young Sun paradox (e.g., *Rondanelli and Lindzen*, 2010; *Goldblatt and Zahnle*, 2011a; see Sect. 7.1 below), for planets at the inner boundary of the habitable zone (e.g., *Kasting*, 1988), and their effect on exoplanet spectroscopy of planets at different ages (e.g., *Kaltenegger et al.*, 2007). The climatic effect of clouds in atmospheres of Earth-like exoplanets and the resulting effects on the potential masking of molecular absorption bands in the planetary spectra has been studied again recently by, e.g., *Kitzmann et al.* (2010, 2011a, 2011b, 2013), *Zsom et al.* (2012), *Rugheimer et al.* (2013), and *Vasquez et al.* (2013a, 2013b).

The impact of clouds on the climate of particular exoplanets is, however, difficult to evaluate without observational constraints on their cloud cover or all the microphysical details (e.g., condensation nuclei) which determine the cloud particle sizes and shapes (*Marley et al.*, 2013).

Active M dwarfs or even young solar-like stars may exhibit strong stellar cosmic-ray emissions. So-called air shower events lead to secondary electron emissions which can break up strong atmospheric molecules like N₂. This can perturb the atmospheric photochemistry, hence affect biosignature molecules and their detectability (see, e.g., *Segura et al.* (2010) and *Grenfell et al.* (2007, 2012) for a discussion on the effect on ozone and other spectral biosignatures). Results suggest for the extreme “flaring case” (see also Sect. 4.5) that ozone may be strongly removed by cosmic ray induced NO_x (*Grenfell et al.*, 2012) whereas the nitrous oxide biosignature may survive. Again, this illustrates the importance of characterizing stellar activity when discussing atmospheric molecular signatures.

5.2 Upper Atmosphere XUV Heating and IR-Cooling

Planets irradiated by high XUV radiation experience heating of the upper atmosphere, related expansion and thermal escape. Ionizing XUV radiation at short wavelengths ($\lambda \leq 102.7$ nm) and dissociating radiation (UV) as well as chemical heating in exothermic 3-body reactions are responsible for the heating of the upper planetary atmospheres (e.g., *Lammer*, 2013). The volume heat production rate q caused by the absorption of the stellar XUV radiation can then be written as (e.g., *Erkaev et al.*, 2013; *Lammer et al.*, 2013b)

$$q_{\text{XUV}} = \eta n \sigma_a J e^{-\tau}, \quad (13)$$

with the energy flux related to the corresponding wavelength range outside the atmosphere, J , the absorption cross-section of atmospheric species, σ_a , the optical depth, τ , and the number density, n . In today’s Venus’ or Earth’s atmosphere, thermospheric heating processes occur near the homopause in the lower thermosphere, where the eddy diffusion coefficient is equal to the molecular diffusion coefficient, at an altitude of ~ 110 km (e.g., *von Zahn et al.*, 1980). Depending on the availability of the main atmospheric constituents and minor species, the thermospheric temperature can be reduced by IR emission in the vibrational-rotational bands of molecules such as CO₂, O₃, H₃⁺, etc.

The fraction of the absorbed stellar XUV radiation transformed into thermal energy is the so-called heating efficiency η ; it lies in the range of ~ 15 –60% (*Chassefière*, 1996a; *Yelle*, 2004; *Lammer et al.*, 2009; *Koskinen et al.*, 2013). Recent calculations by *Koskinen et al.* (2013) estimate the total heating rate based on the absorption of stellar XUV radiation, photoelectrons and photochemistry for the hydrogen-rich “hot Jupiter” HD 209458b with an orbit of 0.047 AU around a solar like star; they found that the heating efficiency for XUV fluxes ~ 450 times today’s solar flux at 1 AU is most likely between ~ 40 –60%. For hydrogen-rich exoplanets exposed to such high XUV fluxes most molecules such as H₂ in the thermosphere are dissociated; thus, IR cooling via H₃⁺ produced by photochemical reactions with H₂ molecules becomes less important (*Koskinen et al.*, 2007). However, depending on the availability of IR-cooling molecules in planetary atmospheres at larger orbital distances exposed to lower XUV fluxes, the heating efficiency may be closer to the lower value of $\sim 15\%$.

5.3 XUV Induced Thermal Atmospheric Escape

Tian et al. (2008) studied the response of Earth’s upper atmosphere to high solar XUV fluxes in more detail and discovered that one can classify the thermosphere response into two thermal regimes. In the first regime, the thermosphere is in hydrostatic equilibrium. In this stage the bulk atmosphere below the exobase can be considered as static similar to the thermospheres of the solar system planets today. However, if the star’s EUV flux was/is much higher

than that of the present Sun, or if the planet’s atmosphere is hydrogen-rich (Watson *et al.*, 1981), the thermosphere can enter a second regime. There, the upper atmosphere is heated to such temperatures that the thermosphere becomes non-hydrostatic. In the hydrodynamic flow regime, the major gases in the thermosphere can expand very efficiently to several planetary radii above the planetary surface. As a result light atoms experience high thermal escape rates and expand to large distances.

In the hydrostatic regime the upper atmosphere experiences classical Jeans escape where particles populating the high-energy tail of a Maxwell distribution at the exobase level have escape energy so that they are lost from the planet. The so-called Jeans parameter, $\lambda_J(r)$, can generally be expressed as (e.g., Chamberlain, 1963)

$$\lambda_J(r) = \frac{GM_{\text{pl}}m}{rkT(r)}, \quad (14)$$

with the gravitational constant G , the planetary mass M_{pl} , the mass of an atmospheric species m , the Boltzmann constant k , and the upper atmosphere temperature T as a function of planetary distance r . As long as $\lambda(r)$ is > 30 , an atmosphere is bound to the planet. For lower values, thermal escape occurs and can become very high if $\lambda(r) \sim 2\text{--}3.5$ (Volkov and Johnson, 2013), depending on the atmospheric main species, the XUV flux, and planetary parameters.

In the non-hydrostatic regime, still not all atoms may reach escape velocity at the exobase level. In such cases one can expect hydrodynamically expanding thermospheres where the loss of the upward flowing atmosphere results in a strong Jeans-type or controlled hydrodynamic escape but not in hydrodynamic blow-off where no control mechanism influences the escaping gas.

Only for $\lambda(r) < 1.5$ does hydrodynamic blow-off occur, and the escape becomes uncontrolled. This happens when the mean thermal energy of the gases at the exobase level exceeds their gravitational energy. Hydrodynamic blow-off can be considered as the most efficient atmospheric escape process. In this extreme condition, the escape is very high because the whole exosphere evaporates and will be refilled by the upward flowing planetary gas of the dynamically expanding thermosphere as long as the thermosphere can remain in this extreme condition. In such cases the thermosphere starts, accompanied by adiabatic cooling, to dynamically expand to several planetary radii (Sekiya *et al.*, 1980; Watson *et al.*, 1981; Chassefière, 1996a; Tian *et al.*, 2005, 2008; Kulikov *et al.*, 2007).

To study the atmospheric structure of an upward flowing, hydrodynamically expanding thermosphere, one has to solve the set of the hydrodynamic equations. For exoplanets orbiting very close to their host stars, one cannot neglect external forces such as gravitational effects related to the Roche lobe (Penz *et al.*, 2008).

5.4 XUV Powered Escape of H-Rich Protoatmospheres

The most efficient atmospheric escape period starts after the planetary nebula dissipated and the protoplanet with its

nebula-captured hydrogen-dominated envelope is exposed to the extreme radiation and plasma environment of the young star. The time period of this extreme escape process depends generally on the host star’s evolving XUV flux, the planet’s orbit location, its gravity, and the main atmospheric constituents in the upper atmosphere. Some planets can be in danger of being stripped of their whole atmospheres; on the other hand, if the atmospheric escape processes are too weak, a planet may have problems getting rid of its protoatmosphere (Lammer *et al.*, 2011b, 2011c; Lammer, 2013; Erkaev *et al.*, 2013; Kislyakova *et al.*, 2013). Both scenarios will have essential implications for habitability.

That the early atmospheres of terrestrial planets were even hydrogen-dominated or contained more hydrogen than nowadays was considered decades ago by researchers such as Holland (1962), Walker (1977), Ringwood (1979), Sekiya *et al.* (1980, 1981), Watson *et al.* (1981), and more recently by Ikoma and Genda (2006). The capture or accumulation of hydrogen envelopes depends on the planetary formation time, the nebula dissipation time, the depletion factor of dust grains in the nebula, the nebula opacity, orbital parameters of other planets in a system, the gravity of the protoplanet, its orbital location, as well as the host star’s radiation and plasma environment (e.g., Ikoma and Genda, 2006; Rafikov, 2006). Depending on all of these parameters, theoretical studies let us expect that fast growing terrestrial planets from Earth to “super-Earth”-type may capture from tens to hundreds or even several thousands of Earth ocean equivalent amounts of hydrogen around their rocky cores (e.g., Hayashi *et al.*, 1979; Mizuno, 1980; Wuchterl, 1993; Ikoma *et al.*, 2000; Ikoma and Genda, 2006; Rafikov, 2006), making them really “mini-Neptunes”. The recent discoveries of “mini-Neptunes” with known sizes and masses indicate that many of them have rocky cores surrounded by a significant amount of hydrogen envelopes (e.g., Lissauer *et al.*, 2011; Erkaev *et al.*, 2013, 2014; Kislyakova *et al.*, 2013; Lammer, 2013).

Adams *et al.* (2008), Mordasini *et al.* (2012), and Kipping *et al.* (2013) studied the mass-radius relationship of planets with primordial hydrogen envelope. The H envelope mass fraction can be written as

$$f = \frac{M_{\text{atm}}}{M_{\text{atm}} + M_{\text{core}}}, \quad (15)$$

with atmosphere mass M_{atm} and core mass M_{core} . Their results indicate that for a given mass, there is a considerable diversity of radii, mainly due to different bulk compositions, reflecting different formation histories. According to Mordasini *et al.* (2012) a protoplanet inside the habitable zone at 1 AU, with $T_{\text{eff}} = 250$ K, with a core mass of $1M_{\oplus}$ and a hydrogen envelope mass fraction f of ~ 0.01 could have a radius of about $\sim 2R_{\oplus}$ depending on its age, orbital distance and activity of its host star.

Additional to such nebula-based hydrogen envelopes, catastrophically outgassed volatile-rich steam atmospheres which depend on the impact history and the initial volatile content of a planet’s interior could also be formed after a

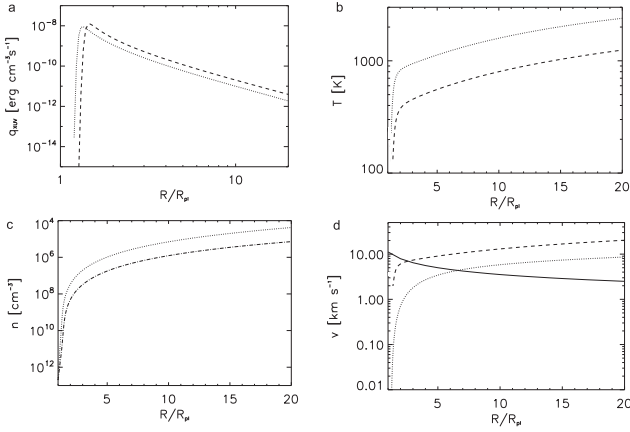


Fig. 8.— Profiles of the volume heating rate (a), thermosphere temperature (b), atmospheric density (c) and outflow velocity (d) as a function of altitude, for an atomic-hydrogen dominated upper atmosphere of an Earth-like planet with a heating efficiency of 15%, subject to an XUV exposure 100 times the present Sun’s at 1 AU. The dotted and dashed lines correspond to a temperature T_{eff} of 250 K at the base of the thermosphere with a lower thermosphere near the planetary surface (dotted line) and one for a hydrogen-dominated protoatmosphere with an envelope mass fraction f of 0.01 and a corresponding radius of $2R_{\oplus}$ (Mordasini *et al.*, 2012). The solid line in (d) corresponds to the escape velocity as a function of distance.

planet finished its accretion (e.g., *Elkins-Tanton and Seager*, 2008; *Elkins-Tanton*, 2011). *Zahnle et al.* (1988) studied the evolution of steam atmospheres as expected on the early Earth and found for surface temperatures close to 2000 K atmospheric temperatures of the order of ~ 1000 K. Recently, *Lebrun et al.* (2013) studied the lifetime of catastrophically outgassed steam atmospheres of early Mars, Earth and Venus and found that water vapor condenses to an ocean after 0.1, 1.5, and 10 Myr, respectively. *Hamano et al.* (2013) defined two planet categories: a type I planet formed beyond a certain critical distance from the host star, solidifying, in agreement with *Lebrun et al.* (2013), within several million years; and type II planets formed inside the critical distance where a magma ocean can be sustained for longer time periods of up to 100 Myr, even with a larger initial amount of water.

Fig. 8 compares the hydrodynamically expanding hydrogen-dominated thermosphere structure for two cases: an Earth-like planet with T_{eff} of 250 K, located within a G-star habitable zone at 1 AU, exposed to an XUV flux 100 times the present-day Sun’s on the one hand, and a similar planet (dashed line) with a more extended nebular-based hydrogen envelope mass fraction of ~ 0.01 with a corresponding radius of $\sim 2R_{\oplus}$ (Mordasini *et al.*, 2012), on the other hand.

For both scenarios shown in Fig. 8 the transonic points are reached below the exobase levels so that the considered atmospheres are in the controlled hydrodynamic regime.

The thermal escape rate with a heating efficiency of 15% for the case where the base of the thermosphere is close to

the planetary radius is $\sim 3.3 \times 10^{31} \text{ s}^{-1}$; for the hydrogen-dominated protoatmosphere with $f = 0.01$ and the corresponding radius at $\sim 2R_{\oplus}$, it is $\sim 5.0 \times 10^{32} \text{ s}^{-1}$. The total losses of hydrogen in equivalent amounts of Earth ocean contents ($1 \text{ EO}_{\text{H}} \sim 1.5 \times 10^{23} \text{ g}$) for the first 100 Myr would be $\sim 1 \text{ EO}_{\text{H}}$ for the case with the smaller lower thermosphere distance and $\sim 15.5 \text{ EO}_{\text{H}}$ for the extended hydrogen dominated protoatmosphere.

One can see from these results that an equivalent amount of only a few EO_{H} may be lost during the first 100 Myr (when the stellar XUV radiation is saturated at high levels); one may expect that terrestrial planets growing rapidly to Earth-mass or “super-Earth-mass” bodies inside the nebula may have a problem with losing their captured hydrogen envelopes. Some planets may keep tens, hundreds or even thousands of EO_{H} (Lammer, 2013; Lammer *et al.*, 2013b).

It is obvious that early Venus or Earth did not capture such huge amounts of nebula gas and most likely did not accrete so fast by collisions with planetary embryos after the nebula disappeared (Albarède and Blichert-Toft, 2007).

For all atmospheric escape processes the age of the host star and planet as well as the host star’s activity are very important. After the planet’s origin, the briefly discussed hydrodynamic expansion and outflow due to the extreme stellar and protoplanetary conditions result in the most efficient atmospheric escape process. During this phase no intrinsic planetary magnetic field will protect the expanded upper atmosphere from ion erosion by the stellar wind. The hydrodynamic outflow changes with decreasing XUV flux and cooling of the lower thermosphere from the hydrodynamic to the hydrostatic regime. For this later phase, a recent study by *Kislyakova et al.* (2013) indicates that stellar wind induced ion pick-up of light species such as atomic hydrogen is always less efficient than thermal escape. However, after the XUV flux of a young and active host star decreases to more moderate XUV flux levels < 5 times that of the present solar value, non-thermal escape processes such as ion pick-up, detached plasma clouds, sputtering, and photochemical losses especially for planets with low gravity become relevant for heavier atmospheric species such as oxygen, carbon and nitrogen.

6. MAGNETOSPHERIC PROTECTION

As a consequence of upper-atmospheric heating by soft X-rays and EUV radiation, the expanding upper atmospheres may reach and even exceed the boundaries of possible planetary magnetospheres. In this case the upper atmosphere will be directly exposed to the plasma flows of the stellar wind and coronal mass ejections (CMEs) with the consequent loss due to ion pick-up, as well as sputtering, and different kinds of photo-chemical energizing mechanisms, all contributing to *non-thermal* atmospheric mass-loss process (Lundin *et al.*, 2007 and references therein; Lichtenegger *et al.*, 2009; Lammer, 2013, and references therein). As a crucial parameter appears here the size of the planetary magnetosphere. Altogether, this makes the plan-

etary magnetic field, as well as the parameters of the stellar wind (mainly its density n_w and speed v_w) very important for the processes of non-thermal atmospheric erosion and mass-loss of a planet, eventually affecting the whole evolution of its environment and possible habitability.

6.1 The Challenge of Magnetospheric Protection

The magnetosphere acts as an obstacle that interacts with the stellar wind, deflecting it and protecting planetary ionospheres and upper atmospheres against the direct impact of stellar wind plasmas and energetic particles (e.g., cosmic rays). For an efficient magnetospheric protection of a planet, the size of its magnetosphere characterized by the magnetopause stand-off distance R_s should be much larger than the height of the outer layers of the exosphere. The value of R_s is determined by the balance between the stellar wind ram pressure and the planetary magnetic field pressure at the substellar point (Grießmeier *et al.*, 2004; Khodachenko *et al.*, 2007a). In most studies related to exoplanetary magnetospheric protection, highly simplified planetary dipole-dominated magnetospheres have been assumed. This means that only the intrinsic magnetic dipole moment of an exoplanet, \mathcal{M} , and the corresponding magnetopause electric currents (i.e., the "screened magnetic dipole" case) are considered as the major magnetosphere forming factors. In this case, i.e., assuming $B(r) \propto \mathcal{M}/r^3$, the value of R_s has been defined by the following expression (Baumjohann and Treumann, 1997),

$$R_s \equiv R_s^{(dip)} = \left[\frac{\mu_0 f_0^2 \mathcal{M}^2}{8\pi^2 \rho_w \tilde{v}_w^2} \right]^{1/6}, \quad (16)$$

where μ_0 is the diamagnetic permeability of free space, $f_0 \approx 1.22$ is a form-factor of the magnetosphere caused by the account of the magnetopause electric currents, $\rho_w = n_w m$ is the mass density of the stellar wind, and \tilde{v}_w is the relative velocity of the stellar wind plasma which includes also the planetary orbital velocity.

The planetary magnetic field is generated by the magnetic dynamo. The existence and efficiency of the dynamo are closely related to the type of the planet and its interior structure. Limitations of the existing observational techniques make direct measurements of the magnetic fields of exoplanets impossible. Therefore, an estimate of \mathcal{M} from simple scaling laws found from an assessment of different contributions in the governing equations of planetary magnetic dynamo theory (Farrell *et al.*, 1999; Sánchez-Lavega, 2004; Grießmeier *et al.*, 2004; Christensen 2010) is widely used. Most of these scaling laws reveal a connection between the intrinsic magnetic field and rotation of a planet. More recently, Reiners and Christensen (2010), based on scaling properties of convection-driven dynamos (Christensen and Aubert, 2006), calculated the evolution of average magnetic fields of "Hot Jupiters" and found that (a) extrasolar gas giants may start their evolution with rather high intrinsic magnetic fields, which then decrease dur-

ing the planet lifetime, and (b) the planetary magnetic moment may be independent of planetary rotation (Reiners and Christensen, 2010). In the case of *rotation-dependent* dynamo models, the estimations of \mathcal{M} give rather small values for tidally locked close-orbit exoplanets, resulting in small sizes of dipole-dominated magnetospheres, $R_s = R_s^{(dip)}$, compressed by the stellar wind plasma flow. The survival of planets in the extreme conditions close to active stars is often used as an argument in favor of *rotation-independent* models, or in favor of a generalization of the dipole-dominated magnetosphere model.

Khodachenko *et al.* (2007b) studied the mass loss of the Hot Jupiter HD 209458b due to the ion pick-up mechanism caused by stellar CMEs colliding with the planet. In spite of the sporadic character of the CME-planetary collisions for the moderately active host star it has been shown that the integral action of the stellar CME impacts over the exoplanet's lifetime can produce a significant effect on the planetary mass loss. The estimates of the non-thermal mass loss of a weakly magnetically protected HD 209458b due to stellar wind ion pick-up suggest significant and sometimes unrealistic values – losses up to several tens of planetary masses M_p during a planet's life time (Khodachenko *et al.*, 2007b). Because multiple close-in giant exoplanets exist, comparable in mass and size to Jupiter, and because it is unlikely that all of them began their life as much more (> ten times) massive objects, one may conclude that additional factors and processes must be considered to avoid full planetary destruction.

6.2 Magnetodisk-Dominated Magnetospheres

The magnetosphere of a close-orbit exoplanet is a complex object whose formation depends on different external and internal factors. These factors may be subdivided into two basic groups: (a) *stellar factors*, e.g., stellar radiation, stellar wind plasma flow, stellar magnetic field and (b) *planetary factors*, e.g., the type of planet, its orbital characteristics, its escaping material flow, and its magnetic field. The structure of an exoplanetary magnetosphere depends also on the speed regime of the stellar wind plasma relative the planet (Erkaev *et al.*, 2005; Ip *et al.*, 2004). In particular, for an exoplanet at sufficiently large orbital distance where the stellar wind is super-sonic and super-Alfvénic, i.e., where the ram pressure of the stellar wind dominates the magnetic pressure, a Jupiter-type magnetosphere with a bow shock, magnetopause, and magnetotail is formed. At the same time, in the case of an extremely close orbital location of an exoplanet (e.g., $d < 0.03$ AU for a solar analog), where the stellar wind is still being accelerated and remains sub-magnetosonic and sub-Alfvénic (Ip *et al.*, 2004; Preusse *et al.*, 2005), an Alfvénic wing-type magnetosphere without a shock in the upstream region is formed. The character of the stellar wind impact on the immediate planetary plasma environment and the atmosphere is different for the super- and sub-Alfvénic types of the magnetosphere. Here, we briefly discuss moderately short-orbit giant planets around solar-

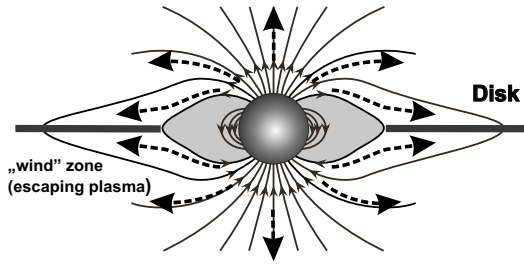


Fig. 9.— Schematic view of magnetodisk formation: The expanding plasma flows along the magnetic field lines and changes the initial dipole topology of the field by the creation of a current disk. In the dead zone (shaded region), plasma is locked by the strong magnetic field; in the wind zone, plasma escapes along the open field lines in the form of an expanding wind.

type stars subject to a super-Alfvénic stellar wind flow, i.e., the magnetospheres having in general a bow shock, a magnetopause, and a magnetotail, similar to Jupiter. Equivalent configurations are expected for Earth-like planets with evaporating atmospheres.

To explain the obvious survival and sufficient magnetospheric protection of close-orbit Hot Jupiters under the extreme conditions of their host stars, *Khodachenko et al.* (2012) proposed a more generic view of a Hot Jupiter magnetosphere. A key element in the proposed approach consists of taking into account the upper atmosphere of a planet as an expanding dynamical gas layer heated and ionized by the stellar XUV radiation (*Johansson et al.*, 2009; *Koskinen et al.*, 2010). Interaction of the outflowing plasma with the rotating planetary magnetic dipole field leads to the development of a current-carrying magnetodisk surrounding the exoplanet. The inner edge of magnetodisk is located at the so called Alfvénic surface ($r = R_A$) where the kinetic energy density of the moving plasma becomes equal to the energy density of the planetary magnetic field (*Havnes and Goertz*, 1984).

Two major regions, separated by the Alfvénic surface at $r = R_A$, with different topologies of the magnetic field may be distinguished in the magnetosphere of a Hot Jupiter driven by the escaping plasma flow (*Mestel*, 1968; *Havnes and Goertz*, 1984). The first region corresponds to the inner magnetosphere, or so-called “dead zone”, filled with closed dipole-type magnetic field lines. The magnetic field in the “dead zone” is strong enough to keep plasma locked with the planet. In the second region, so-called “wind zone”, the expanding plasma drags and opens the magnetic field lines (see Fig. 9). The plasma escaping along field lines beyond the Alfvénic surface not only deforms and stretches the original planetary dipole field, but also creates a thin disk-type current sheet in the equatorial region. Altogether, this leads to the development of a new type of magnetodisk-dominated magnetosphere of a Hot Jupiter, which has no analog among the solar system planets (*Khodachenko et al.*, 2012). It enlarges the magnetospheric obstacle, thus helping to suppress non-thermal escape processes.

6.3 Wind-Exosphere-Magnetosphere Interaction

As discussed before, extended hydrogen exospheres will be produced if hydrogen is the dominating constituent in the upper atmosphere. *Vidal-Madjar et al.* (2003) were the first to observe the transiting exoplanet HD 209458b with the HST/STIS-instrument and discovered a $15 \pm 4\%$ intensity drop in the stellar Lyman- α line in the high velocity part of the spectra. The estimate of the absorption rate has later been carried out independently by *Ben-Jaffel* (2007) who found a lower absorption rate of about $8.9 \pm 2.1\%$, also significantly greater than the transit depth due to the planetary disk alone (*Ben-Jaffel and Sona Hosseini*, 2010). Recently, two other observations of extended upper atmospheres due to Lyman- α absorption during the transits of the short periodic gas giant, HD 189733b, have also been reported (*Lecavelier des Etangs et al.*, 2010, 2012). *Holmström et al.* (2008), *Ekenbäck et al.* (2010) and *Lammer et al.* (2011a) have demonstrated that the exosphere-magnetosphere environment of hydrogen-rich gas giants in orbit locations ≤ 0.05 AU should be strongly affected by the production of energetic neutral H atoms (ENAs) as well as non-thermal ion escape processes.

Similar processes can be expected for EUV-heated and hydrodynamically expanding upper atmospheres of terrestrial exoplanets, where the upper atmosphere can expand beyond possible magnetopause configurations so that ENAs will be produced via charge exchange between the charged stellar wind plasma flow and the exospheric particles. From the ionization of exospheric planetary neutral atoms one can probe of the stellar wind induced ion pick-up loss rate. Recently, *Kislyakova et al.* (2013) applied a stellar wind plasma flow and upper atmosphere interaction model to hydrogen-rich terrestrial planets, exposed to an EUV flux 100 times the present solar strength within the habitable zone of a typical M-star at ~ 0.24 AU. This study found non-thermal escape rates of $\sim 5 \times 10^{30} \text{ s}^{-1}$, which is about one order of magnitude weaker than the EUV-driven thermal escape rates.

As one can see from Fig. 10 the hydrogen atoms populate a wide area around the planet. The EUV flux is deposited mainly in the lower thermosphere, while the fraction of the ENAs which are directed towards the planet should be deposited in an atmospheric layer below the exobase level where they contribute to thermospheric heating. The production of such huge hydrogen coronae and related ENAs was predicted by *Chassefière* (1996a) when he studied the hydrodynamic escape of hydrogen from a hot H₂O-rich early Venus thermosphere. This author suggested that the production of ENAs under such extreme conditions should make an important contribution to the heat budget in the upper atmosphere. The expected energy deposition to hydrodynamically expanding but adiabatically cooling upper atmospheres has to be studied in the future because this important stellar wind-plasma induced feedback process can rise the temperature to higher values than the EUV radiation, thus possibly enhancing thermal escape.

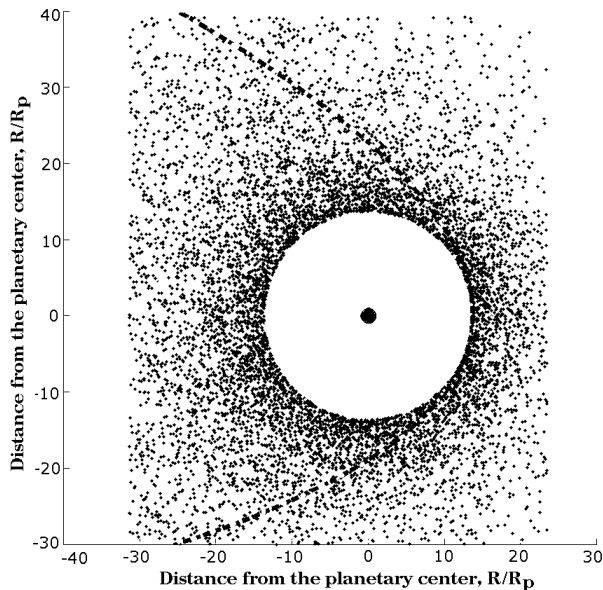


Fig. 10.— Modeled extended neutral atomic hydrogen exosphere around a hydrogen-rich “super-Earth” inside an M star HZ at 0.24 AU with the size of $2R_{\oplus}$ and $10M_{\oplus}$; the EUV flux is 50 times the present Sun’s. The stellar wind plasma density and velocity are $\sim 250 \text{ cm}^{-3}$ and 330 km s^{-1} , respectively. The small dots represent the neutral hydrogen atoms, the big dot in the center represents the planet (after *Kislyakova et al.*, 2013).

7. APPLICATIONS

7.1 The Faint Young Sun Paradox

Stellar evolution theory indicates that the ZAMS Sun was fainter by about 30% than the present-day Sun; the radiative output has increased gradually since then (Sect. 4.1). Estimates of the Earth’s and Mars’ surface temperatures in the presence of their modern atmospheres indicate that both should have been at average temperatures much below the freezing point of liquid water (*Sagan and Mullen*, 1972). Geological evidence, however, clearly suggests warm climates in the first billion years, and the presence of liquid water (*Kasting and Toon*, 1989; *Valley et al.*, 2002; *Feulner*, 2012). Without some source of additional warming, the Earth’s surface temperature should not have risen above the freezing point until about 2 billion years ago, long after the first traces of life on Earth appeared (*Kasting and Catling*, 2003). This apparent contradiction is known as the “Faint Young Sun Paradox” (FYSP).

The FYSP has several different possible solutions, and it is not yet agreed which, if any of these, is correct. These solutions fall into three basic categories:

- *Additional greenhouse gases.* Higher levels of greenhouse gases could raise the atmospheric temperatures significantly (important also in the present-day Earth’s atmosphere). For the Earth, increased levels of atmospheric CO_2 together with water vapor would potentially suffice, and the

CO_2 level could even self-regulate the mild climate through the carbonate-silicate cycle (*Walker et al.*, 1981). However, geological evidence from paleosols (*Sheldon*, 2006; *Driese et al.*, 2011) argues against massively increased CO_2 levels on the young Earth.

Previous paleosol constraints published by *Rye et al.* (1995) have been criticized (*Sheldon*, 2006), as have the very low CO_2 estimates from banded iron-formations published by *Rosing et al.* (2010) (*Reinhard and Planavsky*, 2011; *Dauphas and Kasting*, 2011). The *Sheldon* and *Driese et al.* CO_2 estimates should be regarded as highly uncertain, as they depend on poorly known factors such as soil porosity and moisture content. Furthermore, recent 3-D climate calculations by *Kienert et al.* (2012) suggest that CO_2 partial pressures on the early Earth must have been even higher than previously calculated (see also in 1D models *Haqq-Misra et al.*, 2008; *von Paris et al.*, 2008), because ice albedo feedback tends to amplify the cold temperatures predicted when CO_2 is low. All of this suggests that additional greenhouse gases were probably needed.

Other greenhouse gases such as NH_3 may dissociate rapidly (*Kuhn and Atreya*, 1979), and CH_4 may form hazes, increasing the albedo, unless at least an equal amount of CO_2 is present (*Haqq-Misra et al.*, 2008). Ethane (C_2H_6) and carbonyl sulfide (OCS) have been proposed as efficient greenhouse gases in the young terrestrial atmosphere (*Haqq-Misra et al.*, 2008; *Ueno et al.*, 2009). Another candidate is N_2O which can build up biotically to quite large concentrations and act as a strong greenhouse gas (*Buick*, 2007; *Roberson et al.*, 2011; *Grenfell et al.*, 2011).

Calculations by *Ramirez et al.* (2014) suggest that the early Mars climate problem could instead be resolved by adding 5–20% H_2 to the atmosphere, as has been suggested recently for early Earth (*Wordsworth and Pierrehumbert*, 2013). In addition, higher partial pressures of N_2 might enhance the effectiveness of the CO_2 greenhouse effect, on both early Earth and early Mars (*Li et al.*, 2009; *Goldblatt et al.*, 2009; *von Paris et al.*, 2013). Furthermore, SO_2 has been investigated for early Mars climate studies (*Postawko and Kuhn*, 1986; *Tian et al.*, 2010; *Mischna et al.*, 2013).

- *Lower albedo.* A planet’s albedo could be changed by lower cloud coverage in particular in cooler environments (*Rossow et al.*, 1982). Detailed studies of clouds show two competing effects (*Goldblatt & Zahnle*, 2011a; *Zsom et al.*, 2012): Low-lying clouds reflect solar radiation, thus increasing the albedo; in contrast, high clouds, in particular ice-crystal cirrus clouds, add to atmospheric greenhouse warming, potentially sufficient to solve the FYSP (*Rondanelli & Lindzen*, 2010) although requiring full coverage by an unrealistically thick and cold cloud cover (*Goldblatt & Zahnle*, 2011a).

A lower surface albedo could be the result of the suggested smaller continental area in early epochs although feedback on cloud coverage may result in opposite trends. The absence of cloud condensation nuclei induced biologically (*Charlson et al.* 1987) also decreases the albedo. Considering these effects and claiming less reflective clouds

because of larger cloud droplets (because of fewer biogenically induced condensation nuclei), *Rosing et al.* (2010) inferred a clement climate for the young Earth without need of high amounts of greenhouse gases (*Rosing et al.*, 2010) although this solution was again questioned (*Goldblatt and Zahnle*, 2011b).

- *A brighter young Sun.* If the Sun had been slightly more massive at arrival on the ZAMS, then its luminosity would have exceeded standard estimates, owing to the $L \propto M^3$ dependence of a cool star’s luminosity, L , on the stellar mass, M . The excess mass could have been shed by a much stronger solar wind in the early phases of solar evolution (*Whitmire et al.*, 1995; *Sackmann and Boothroyd*, 2003). This hypothesis is constrained by the requirement that Martian temperatures be supportive of liquid water, while preventing a runaway greenhouse on Earth. The resulting ZAMS mass of the Sun would then be 1.03–1.07 M_{\odot} (*Sackmann and Boothroyd*, 2003). Upper limits to the ionized-wind mass-loss rates deduced from radio observations of young solar analogs are marginally compatible with the “Bright Young Sun” requirement, indicating a maximum ZAMS solar mass of 1.06 M_{\odot} (*Gaidos et al.*, 2000). Estimates of the young Sun’s wind mass-loss, however (Sect. 4.4), suggest a total main-sequence mass-loss of the Sun of only 0.3% (*Minton and Malhotra*, 2007), too little to explain the FYSP.

7.2 Venus Versus Earth

The atmosphere of present Venus is extremely dry when compared to the terrestrial atmosphere (a total water content of 2×10^{19} g or 0.0014% of the terrestrial ocean, vs. 1.39×10^{24} g on Earth; *Kasting and Pollack*, 1983). The similar masses of Venus and Earth and their formation at similar locations in the solar nebula would suggest that both started with similar water reservoirs (*Kasting and Pollack*, 1983). Terrestrial planets such as Venus, Earth and Mars, with silicate mantles and metallic cores, most likely obtain water and carbon compounds during their accretion (see Sect. 3). The largest part of a planet’s initial volatile inventory is outgassed into the atmosphere during the end of magma ocean solidification (e.g., *Zahnle et al.*, 1988, 2007; *Elkins-Tanton*, 2008; *Lebrun et al.*, 2013; *Hamano et al.*, 2013; *Lammer*, 2013). Only a small fraction of the initial volatile inventory will be released into the atmospheres through volcanism. From estimates by considering the possible range of the initial water content in the building blocks of Venus and Earth it appears possible that both planets may have outgassed hot steam atmospheres with surface pressures up to ~ 500 bar (*Elkins-Tanton*, 2008).

Recently, *Lebrun et al.* (2013), studied the thermal evolution of early magma oceans in interaction with outgassed steam atmospheres for early Venus, Earth and Mars. Their results indicate that the water vapor of these steam atmospheres condensed to an liquid ocean after ~ 10 , 1.5 and 0.1 Myr for Venus, Earth and Mars, respectively, and remained in vapor form for Earth-type planets orbiting closer than

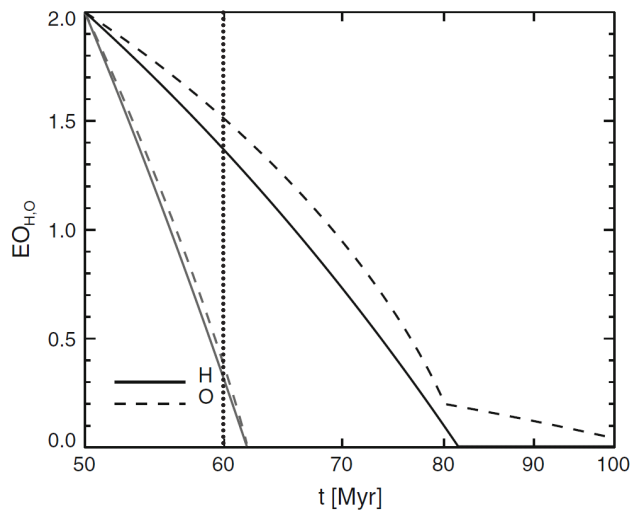


Fig. 11.— Hydrodynamic loss of atomic hydrogen and dragged oxygen atoms from a 500 bar outgassed, dissociated steam atmosphere on early Venus during the young Sun’s EUV saturation phase (100 times the present EUV flux). The black and grey lines correspond to heating efficiencies of 15% and 40%, respectively (after *Lammer*, 2013). The dotted line marks the time when the steam atmosphere may have condensed (*Lebrun et al.*, 2013) so that an ocean could have formed on the planet’s surface.

0.66 AU around a solar-like star. However, these authors point out that their results depend on the chosen opacities and it is conceivable that no liquid oceans formed on early Venus. This possibility is also suggested by *Hamano et al.* (2013) who studied the emergence of steam atmosphere-produced water oceans on terrestrial planets.

The critical solar flux leading to complete evaporation of a water ocean (a “runaway greenhouse”, *Ingersoll*, 1969) is $\approx 1.4 S_{\text{sun}}$ nearly independently of the amount of cooling CO_2 in the atmosphere (*Kasting*, 1988), where $S_{\text{sun}} = 1360 \text{ Wm}^{-2}$ is the present-day solar constant. This critical flux is just about the flux expected from the young Sun at the orbit of Venus (and is about 70% of the present-day value at the same solar distance). New calculations by *Kopparapu et al.* (2013) give a runaway greenhouse limit of $1.06 S_{\text{sun}}$. That limit, however, like the *Kasting* (1988) value before it, is almost certainly too low, because it assumes a fully saturated atmosphere and it neglects cloud feedback.

Venus’ atmosphere also reveals a surprisingly high deuterium-to-hydrogen (D/H) abundance ratio of $(1.6 \pm 0.2) \times 10^{-2}$ or 100 times the terrestrial value of 1.56×10^{-4} (*Kasting and Pollack*, 1983). These observations have motivated a basic model in which water was abundantly available on the primitive Venus. Any water oceans would evaporate, inducing a “runaway greenhouse” in which water vapor would become the major constituent of the atmosphere. This vapor was then photodissociated in the upper atmosphere by enhanced solar EUV irradiation (*Kasting and Pollack*, 1983) as well as by frequent meteorite im-

pacts in the lower thermosphere (*Chassefière, 1996b*), followed by the escape of hydrogen into space (*Watson et al., 1981; Kasting and Pollack, 1983; Chassefière, 1996a, 1996b; Lammer et al., 2011c*). During the phase of strong thermal escape of atomic hydrogen, remaining oxygen and similar species can be dragged to space by the outward flowing hydrogen flux (*Hunten et al., 1987; Zahnle and Kasting, 1986; Chassefière, 1996a, 1996b; Lammer et al., 2011c*).

Fig. 11 shows the hydrodynamic escape of a hypothetical 500 bar steam atmosphere from early Venus exposed to an EUV flux 100 times the present solar value, for assumed heating efficiencies of 15% and 40% (*Lammer et al., 2011c; Lammer, 2013*). In this scenario, it is assumed that early Venus finished its accretion ~ 50 Myr after the origin of the Sun and outgassed the maximum expected fraction of its initial water inventory after the magma ocean solidified. One can see that the whole steam atmosphere could have been lost within the condensation time scale of about 10 Myr modeled by *Lebrun et al. (2013)* for a heating efficiency of 40% as estimated for “Hot Jupiters” (*Koskinen et al., 2013*). For a heating efficiency of 15% (e.g., *Chassefière, 1996a, 1996b*) and assuming that the outgassed steam atmosphere remains in vapor form, the planet would have lost its hydrogen after ~ 30 Myr, leaving behind some of its oxygen. If the remaining O atoms also experienced high thermal escape rates during the remaining high EUV phase, they would be lost by a combination of thermal and non-thermal escape processes (*Lundin et al., 2007*). If the high-density CO₂ lower thermosphere was efficiently cooled down to suppress high thermal escape rates of oxygen, the remaining oxygen in the upper atmosphere could have been lost by non-thermal escape processes such as solar wind induced ion pick-up and cool ion outflow (e.g., *Kulikovic et al., 2006; Lundin et al., 2007; Lammer, 2013*).

If the steam atmosphere cooled within ~ 10 Myr, so that the remaining water vapor could condense, then a liquid water ocean may have formed on Venus’ surface for some period before it again evaporated by the above mentioned “runaway greenhouse” effect. On the other hand, if early Venus degassed an initial water content that resulted in a steam atmosphere with < 250 bar, then the water would most likely have been lost during its vapor phase so that an ocean could never form on the planet’s surface.

As discussed in *Lammer et al. (2011c)* and studied in detail in *Lebrun et al. (2013)* and *Hamano et al. (2013)*, the outgassed steam atmosphere of the early Earth cooled faster because of its larger distance from the Sun, and this resulted in a shorter condensation time scale compared to the escape. Therefore, a huge fraction of the water vapor condensed and produced Earth’s early ocean.

7.3 Mars

Latest research on the formation of Mars indicates that the body formed within ~ 5 Myr and remained as a planetary embryo that never accreted toward a larger planet

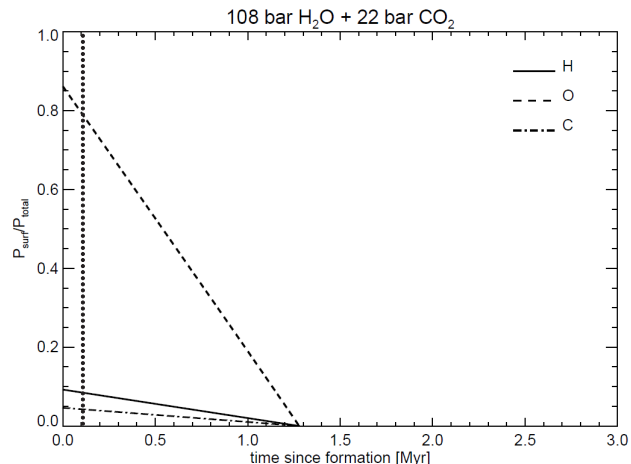


Fig. 12.— Hydrodynamic loss of atomic hydrogen and dragged oxygen and carbon atoms from an outgassed and dissociated steam atmosphere (108 bar H₂O, 22 bar CO₂) on early Mars during the young Sun’s EUV saturation phase (100 times the present solar EUV level; after *Erkaev et al., 2014*). The dotted line marks the time period when the steam atmosphere may have condensed (*Lebrun et al., 2013*), so that an ocean could have formed on the planet’s surface (neglecting the energy deposited at the planet’s surface by frequent planetesimal impacts and small embryos).

(*Brasser, 2013*). From the building blocks and their water contents expected in the Martian orbit, it is estimated that early Mars catastrophically outgassed volatiles amounting to ~ 50 – 250 bar of H₂O and ~ 10 – 55 bar of CO₂, after the solidification of its magma ocean (*Elkins-Tanton, 2008*). As shown in Fig. 12, due to the high EUV flux of the young Sun, such a steam atmosphere was most likely lost via hydrodynamic escape of atomic hydrogen, dragging heavier atoms such as C and O during the first million years after the magma ocean solidified (*Lammer et al., 2013c; Erkaev et al., 2014*). Although *Lebrun et al. (2013)* found that a degassed steam atmosphere on early Mars would condense after ~ 0.1 Myr, frequent impacts of large planetesimals and small embryos during the early Noachian most likely kept the protoatmosphere in vapor form (*Lammer et al., 2013c*). After early Mars lost its outgassed protoatmosphere the atmospheric escape rates were most likely balanced by a secondary outgassed atmosphere and delivered volatiles by impacts until the activity of the young Sun decreased so that the atmospheric sources could dominate over the losses (*Tian et al., 2009; Lammer et al., 2013c*). There is substantial evidence for a warmer and wetter climate on ancient Mars ~ 3.5 – 4 Gyr ago (e.g., *Carr and Head, 2003*). Mantle outgassing and impact-related volatiles may have resulted in the buildup of a secondary CO₂ atmosphere of a few tens to a few hundred mbar around the end of the Noachian (*Grott et al., 2011; Lammer et al., 2013c*). The evolution of the planet’s secondary atmosphere and its water content during the past 4 Gyr was most likely determined by an interplay of non-thermal atmospheric escape processes

such as direct escape of photochemically hot atoms, atmospheric sputtering, ion pick-up and cool ion outflow as well as impacts (e.g., *Lundin et al.*, 2007; *Lammer et al.* 2013c and references therein), carbonate precipitation, and serpentinization (*Chassefière and Leblanc*, 2011a, 2011b; *Chassefière et al.*, 2013) which finally led to the present-day environmental conditions.

8. THE VARIETY OF HABITABLE CONDITIONS

With the rapidly increasing number of detected exoplanetary systems, the diversity of system architectures, sizes and radii of the individual planets and the range of average planetary densities have come into the focus of *planetary characterization*. It is by now clear that a much wider range of planetary characteristics is realized in exoplanetary systems than available in the solar system. Hot Jupiters, massive planets in habitable zones, resonant systems, planets in highly eccentric orbits, and small planets with very low average densities (below that of water) are challenging planetary formation, migration, and evolution theories.

Whether a planet is ultimately habitable depends on a surprisingly large number of astrophysical and geophysical factors, of which we have reviewed the former here. The correct distance from the host star is the most obvious and defining parameter for a habitable zone, but it provides by no means a sufficient condition for habitability. Migration and resonant processes in the young planetary systems are crucial for the fate of stable orbits of potentially habitable planets. In what looks like a tricky paradox, water is not available in solids in the very region where habitable zones evolve around cool stars; rather, water needs to be brought there, and gas giant planets may have to do the job of stirring the orbits of the outer planetesimals to scatter them to regions where water is scarce. Water transport through collisions is itself a difficult process, as water needs to survive such collisions to accumulate in the required amounts on the forming planet. Atmospheres outgassed from the planet and trapped from the early protoplanetary disk wrap the growing planet into an extremely dense envelope that itself defies habitability but may be protective of forming secondary atmospheres. Once atmospheres evolve, the harsh environment of the young star begins to act severely. EUV and X-ray radiation hundreds to thousands of times stronger than the present-day Sun's and stellar winds up to hundreds of times stronger than at present begin to erode upper atmospheres of planets, in particular if no magnetosphere is present that may sufficiently protect the atmosphere. Ultraviolet emission determines the atmospheric temperature profiles and induces a rich chemistry that may become relevant for the formation of life. Here, host star spectral type matters for the formation of an atmospheric temperature inversion. An abiotically forming ozone layer may be one of the important results especially for active M dwarfs.

The outcome may be an extremely rich variety of potentially habitable environments, but we still lack thorough knowledge of all relevant factors that really determine hab-

itability. While M dwarfs have become favored targets to search for planets in their habitable zones, such planets may be affected by the strong, long-term high-energy radiation and harsh wind conditions for too long to actually develop habitable planetary surfaces. Their atmospheres may be subject to excessively strong erosion processes.

On the other hand, the development of two habitable planets in the solar system, at least one with thriving life, provides ample evidence that some of the risks, e.g., too heavy protoatmospheres or too rapid erosion of early nitrogen atmospheres, were successfully overcome (*Lammer et al.*, 2013a). One wonders if some sort of fine-tuning was at work, for example between the timing of planet formation and disk dispersal, the outgassing history and the eroding high-energy radiation, the presence of giants like Jupiter or Saturn controlling the architecture and stability of planetary orbits in the habitable zone, or the mass- and perhaps rotation-dependent formation of a magnetosphere protecting the upper atmosphere of a planet. If such did not succeed, then habitable-zone planets may end up with huge high-pressure hydrogen atmospheres, suggested by the detection of small, low-density exoplanets, or strongly eroded atmospheres such as on Mars, or the complete loss of their atmospheres. Other planets may be close to habitable zones but may dwell in eccentric orbits, making surface life more problematic.

Apart from the diverse astrophysical conditions, a plethora of *geophysical* conditions matter, such as planetary internal convection and geodynamos, plate tectonics, volcanism, the presence and distribution of land mass, the orientation and stability of the rotation axis, etc. They as well interact with the diverse astrophysical factors discussed in this article, to add further constraints on actual habitability.

Acknowledgments. We thank an anonymous referee for useful comments that helped improve this chapter. M. G., R. D., M. L. K., H. L. and E. P.-L. thank the Austrian Science Fund (FWF) for financial support (research grants related to planetary habitability: S116001-N16 and S116004-N16 for M. G., S11603-N16 for R. D., S116606-N16 for M. L. K., S116607-N16 for H. L., S11608-N16 and P22603-N16 for E. P.-L.). N. V. E. acknowledges support by the RFBR grant No 12-05-00152-a. J. K. thanks the NASA Astrobiology and Exobiology programs. H. R. and H. L. thank for the support by the Helmholtz Association through the research alliance "Planetary Evolution and Life." I. R. acknowledges financial support from the Spanish Ministry of Economy and Competitiveness (MINECO) and the "Fondo Europeo de Desarrollo Regional" (FEDER) through grant AYA2012-39612-C03-01. M. G., H. L., and M. L. K. acknowledge support by the International Space Science Institute in Bern, Switzerland, and the ISSI Team "Characterizing Stellar and Exoplanetary Environments."

REFERENCES

- Abe Y., et al. (2011) *Astrobiol.*, 11, 443-460.
- Adams E. R., et al. (2008) *Astrophys. J.*, 673, 1160-1164.
- Albarède F. and Blichert-Toft J. (2007) *C. R. Geosci.*, 339, 917-927.
- Anglada-Escudé G., et al. (2012) *Astrophys. J.*, 751, id.L16.
- Audard M., et al. (2000) *Astrophys. J.*, 541, 396-409.
- Baraffe I., et al. (1998) *Astron. Astrophys.*, 337, 403-412.
- Baross J. A., et al. (2007) In *Planets and Life: The Emerging Science of Astrobiology* (W. T. I. Sullivan and J. A. Baross, eds) pp. 275-291. Cambridge Univ. Press, Cambridge.
- Batalha N. M., et al. (2011) *Astrophys. J.*, 729, id.27.
- Batalha N. M., et al. (2013) *Astrophys. J. Suppl. Ser.*, 204, id.24.
- Baumjohann W. and Treumann R. A. (1997) *Basic space plasma physics*, Imperial College Press, London.
- Ben-Jaffel L. (2007) *ApJ*, 671, L61-L64.
- Ben-Jaffel L. and Sona Hosseini S. (2010) *ApJ*, 709, 1284-1296.
- Bonfils X., Delfosse X., Udry S., et al. (2013) *Astron. Astrophys.*, 549, A109.
- Borucki W. J., et al. (2013) *Science*, 340, 587-590.
- Brasser R. (2013) *Space Sci. Rev.*, 174, 11-25.
- Buchhave L. A., et al. (2012) *Nature*, 486, 375-377.
- Buick R. (2007) *Geobiol.*, 5, 97-100.
- Carr M. H. and Head J. W. (2003) *J. Geophys. Res.*, 108, 8/1-28, CiteID 5042.
- Chamberlain J. W. (1963) *Planet. Space. Sci.*, 11, 901-996.
- Chapman S. A. (1930) *Mem. R. Met. Soc.*, 3, 103-125.
- Charlson R. J., et al. (1987) *Nature*, 326, 655-661.
- Chassefière E. (1996a) *J. Geophys. Res.*, 101, 26039-26056.
- Chassefière E. (1996b) *Icarus*, 124, 537-552.
- Chassefière E. and Leblanc F. (2011a) *Earth Planet. Sci. Lett.*, 310, 262-271.
- Chassefière E. and Leblanc F. (2011b) *Planet. Space Sci.* 59, 218-226.
- Chassefière E., et al. (2013) *J. Geophys. Res.* 118, 1123-1134.
- Chiang E. I. (2003) *Astrophys. J.*, 584, 465-471.
- Christensen U. R. (2010) *Space Sci. Rev.*, 152, 565-590.
- Christensen U. R. and Aubert J. (2006) *Geophys. J. Int.*, 166, 97-114.
- Claire M. W., et al. (2012) *Astrophys. J.*, 757, id. 95.
- Crutzen P. J. (1970) *Q. J. R. Meteorol. Soc.*, 96, 320-325.
- Dauphas N. and Kasting J. F. (2011) *Nature*, 474, E2-E3.
- Drake S. A., et al. (1993) *Astrophys. J.*, 406, 247-251.
- Driese S. G., et al. (2011) *Precambrian Res.*, 189, 1-17.
- Dvorak R., et al. (2012), in *Let's Face Chaos through Nonlinear Dynamics* (M. Robnik and V. G. Romanovski, eds.), pp. 137-147. American Institute of Physics, Melville, NY.
- Eggl S., et al. (2012) *Astrophys. J.*, 752, 74-85.
- Ekenbäck A., et al., (2010) *Astrophys. J.*, 709, 670-679.
- Elkins-Tanton L. T. (2008) *Earth Planet. Sci. Lett.* 271, 181-191.
- Elkins-Tanton L. T. (2011) *Astrophys. Space Sci.*, 332, 359-364.
- Elkins-Tanton L. and Seager S. (2008) *Astrophys. J.*, 685, 1237-1246.
- Erkaev N. V., et al. (2005) *Astrophys. J. Suppl. Ser.*, 157, 396-401.
- Erkaev N. V., et al. (2013) *Astrobiol.*, 13, 1011-1029.
- Erkaev N. V., et al. (2014) *Planet. Space Sci.*, 98, 106-119. ; changed MG 29 July 2014
- Farrell W. M., et al. (1999) *J. Geophys. Res.*, 104, (E6), 14025-14032.
- Feldman W. C., et al. (1977) In *The Solar Output and its Variation*, (O. R. White, ed.), pp. 351-382. Colorado Associated University Press.
- Fulner G. (2012) *Reviews of Geophysics*, 50, CiteID RG2006.
- Forget F. and Pierrehumbert R. T. (1997) *Science*, 278, 1273-1276.
- France K., et al. (2013) *Astrophys. J.*, 763, id. 149.
- Fressin F., et al. (2013) *Astrophys. J.*, 766, id.81.
- Garcés A., et al. (2011) *Astron. Astrophys.*, 531, A7.
- Gaidos E. J., et al. (2000) *Geophys. Res. Lett.*, 27, 501-503.
- Gayley K. G., et al. (1997) *Astrophys. J.* 487, 259-270.
- Gilliland R. L., et al. (2011) *Astrophys. J. Suppl. Series*, 197, id.6.
- Goldblatt M. T. and Zahnle K.J. (2011a) *Clim. Past*, 7, 203-220.
- Goldblatt M. T. and Zahnle K. J. (2011b) *Nature*, 474, E3-4.
- Goldblatt C., et al. (2009), *Nature Geoscience*, 2, 891-896.
- Grenfell J. L., et al. (2007) *Astrobiol.*, 7, 208-221.
- Grenfell J. L., et al. (2011) *Icarus*, 211, 81-88.
- Grenfell J. L., et al. (2012) *Astrobiol.*, 12, 1109-1122.
- Grenfell J. L., et al. (2013) *Astrobiol.*, 13, 415-438.
- Grenfell J. L., et al. (2014) *Planet. Space Sci.*, 98, 66-76. ; added MG 29 July 2014
- Grießmeier J.-M., et al. (2004) *Astron. Astrophys.*, 425, 753-762.
- Grott M., et al. (2011) *Earth Planet. Sci. Lett.* 308, 391-400.
- Güdel M. (2004) *Astron. Astrophys. Rev.*, 12, 71-237.
- Güdel M. (2007) *Liv. Rev. Solar Phys.*, 4, no. 3; online <http://solarphysics.livingreviews.org/Articles/lrsp-2007-3/>.
- Güdel M., et al. (1997) *Astrophys. J.* 483, 947-960.
- Guinan E. F. and Engle S. G. (2009) In *The Ages of Stars* (E. E. Mamajek, D. R. Soderblom, and R. F. G. Wyse, eds.) *IAU Symp.* 258, 395-408.
- Haagen-Smit A. J., et al. (1952) *2nd Proc. Nat. Air. Symp.*, 54-56.
- Haghighipour N. and Kaltenegger L. (2013) *Astrophys. J.*, 777, id.166.
- Hamano K., et al. (2013) *Nature*, 497, 607-610.
- Haqq-Misra J. D., et al. (2008) *Astrobiol.*, 8, 1127-1137.
- Hart M. H. (1979) *Icarus*, 37, 351-357.
- Havnes O. and Goertz C. K. (1984) *Astron. Astrophys.*, 138, 421-430.
- Hayashi C., et al. (1979) *Earth & Planet. Sci. Lett.*, 43, 22-28.
- Hedelt P., et al. (2013) *Astron. Astrophys.*, 553, idA9.
- Holland H. D. (1962) In *Petrologic studies* (A. E. J. Engel, H. L. James, and B. F. Leonard, eds.) *Geol. Soc. Amer.*, Boulder, Colorado.
- Holmström M., et al. (2008) *Nature*, 451, 970-972.
- Howard A. W. (2013) *Science*, 340, 572-576.
- Hu R., et al. (2012) *Astrophys. J.*, 761, id. 166.
- Hunten D. M., et al. (1987) *Icarus*, 69, 532-549.
- Ikoma M., et al. (2000) *Astrophys. J.*, 537, 1013-1025.
- Ikoma M. and Genda H. (2006) *Astrophys. J.*, 648, 696-706.
- Ingersoll A. P. (1969) *J. Atmospheric Sci.*, 26, 1191-1198.
- Ip W.-H., et al. (2004) *Astrophys. J.*, 602, L53-L56.
- Johansson E. P. G., et al. (2009) *Astron. Astrophys.*, 496, 869-877.
- Kaltenegger L. and Haghighipour N. (2013) *Astrophys. J.*, 777, id.165.
- Kaltenegger L., et al. (2007) *Astrophys. J.*, 658, 598-616.
- Kaltenegger L., et al. (2011) *Astrophys. J.*, 733, id.35.
- Kaltenegger L., et al. (2013) *Astrophys. J.*, 755, id.L47.
- Kane S. R. and Hinkel N. R. (2013) *Astrophys. J.*, 762, id.7.
- Kasting J. F. (1988) *Icarus*, 74, 472-494.
- Kasting J. F. and Catling D. (2003) *Annu. Rev. Astron. Astrophys.*, 41, 429-463.
- Kasting J. F. and Pollack J. B. (1983) *Icarus*, 53, 479-508.
- Kasting J. F. and Toon O. B. (1989) In *Origin and Evolution of Planetary and Satellite Atmospheres*, (S. K. Atreya, J. B. Pol-

- lack, and M. S. Matthews, eds), pp. 423-449, University of Arizona Press, Tucson, USA.
- Kasting J. F., et al. (1993) *Icarus*, 101, 108-128.
- Kasting J. F., et al. (2014) *Proc. Nat. Acad. Sci.*, in press.
- Kharecha P., et al. (2005) *Geobiol.*, 3, 53-76.
- Khodachenko M. L., et al. (2007a) *Astrobiol.*, 7, 167-184.
- Khodachenko M. L., et al. (2007b) *Planet. Space Sci.*, 55, 631-642.
- Khodachenko M. L., et al. (2012) *Astrophys. J.*, 744, 70-86.
- Kienert H., et al. (2012) *Geophys. Res. Lett.* 39, Issue 23, CiteID L23710.
- Kipping D. M., et al. (2013) *Mon. Not. Roy. Astron. Soc.*, 434, 1883-1888.
- Kislyakova G. K., et al. (2013) *Astrobiol.*, 13, 1030-1048.
- Kitzmann D., et al. (2010) *Astron. Astrophys.*, 511, id.A66.
- Kitzmann D., et al. (2011a) *Astron. Astrophys.*, 531, id.A62.
- Kitzmann D., et al. (2011b) *Astron. Astrophys.*, 534, id.A63.
- Kitzmann D., et al. (2013) *Astron. Astrophys.*, 557, id.A6.
- Kopparapu R. K. (2013) *Astrophys. J.*, 767, id.L8.
- Kopparapu R. K., et al. (2013) *Astrophys. J.*, 765, id.131.
- Koskinen T. T., et al. (2007) *Nature*, 450, 845-848.
- Koskinen T., et al. (2010) *Astrophys. J.*, 723, 116-128.
- Koskinen T. T., et al. (2013) *Icarus*, 226, 1678-1694.
- Kuhn W. R. and Atreya S. K. (1979) *Icarus*, 37, 207-213.
- Kulikov Y. N., et al. (2006) *Planet. Space Sci.*, 54, 1425-1444.
- Kulikov Yu. N., et al. (2007) *Space Sci Rev.*, 129, 207-243.
- Lammer H. (2013) *Origin and evolution of planetary atmospheres: Implications for habitability*, Springer Briefs in Astronomy, Springer, pp. 98, Heidelberg/New York.
- Lammer H., et al. (2009) *Astron. Astrophys.*, 506, 399-410.
- Lammer H., et al., (2011a) *Astrophys. Space Sci.*, 335, 9-23.
- Lammer H., et al. (2011b) *Astrophys. Space Sci.*, 335, 39-50.
- Lammer H., et al. (2011c) *Orig. Life Evol. Bisoph.* 41, 503-522.
- Lammer H., et al. (2013a) In: *The early evolution of the atmospheres of terrestrial planets* (J. M. Trigo-Rodriguez, F. Raulin, F., C. Muller, and C. Nixon) *Astrophys. and Space Science Proc.*, pp. 35-52. Springer Verlag, Heidelberg, New York.
- Lammer H., et al. (2013b) *Mon. Not. Roy. Astron. Soc.*, 430, 1247-1256.
- Lammer H., et al. (2013c) *Space Sci. Rev.* 174, 113-154.
- Lebrun T., et al. (2013) *J. Geophys. Res.*, 118, 1-22.
- Lecavelier des Etangs A., et al., (2010) *Astron. Astrophys.*, 514, A72.
- Lecavelier des Etangs A., et al. (2012) *Astron. Astrophys.*, 543, L4.
- Leconte J., et al. (2013) *Astron. Astrophys.*, 554, A69.
- Lederberg J. (1965) *Nature*, 207, 9-13.
- Léger A., et al. (2009) *Astron. Astrophys.*, 506, 287-302.
- Li K., Pahlevan K., et al. (2009) *Proc. Nat. Academy Sci.*, 9576-9579.
- Lichtenegger H. I. M., et al. (2009) *Geophys. Res. Lett.* 36, CiteID L10204.
- Lim J. and White S. M. (1996) *Astrophys. J.*, 462, L91-L94.
- Lim J., et al. (1996) *Astrophys. J.*, 460, 976-983.
- Linsky J. L. and Wood B. E. (1996) *Astrophys. J.*, 463, 254-270.
- Linsky J. L., et al. (2012) *Astrophys. J.*, 745, id. 25.
- Linsky J. L., et al. (2013) *Astrophys. J.*, 766, id. 69.
- Lissauer J. J. and the Kepler Team (2011) *Nature*, 470, 53-58.
- Lovelock J. E. (1965) *Nature*, 207, 568-570.
- Lundin R., et al. (2007) *Space Sci. Rev.*, 129, 245-278.
- Lunine J., et al. (2011) *Adv. Sci. Lett.*, 4, 325-338.
- Maehara H., et al. (2012) *Nature*, 485, 478-481.
- Maindl T. I. and Dvorak, R. (2014), in *IAU Symposium 299: Exploring the formation and evolution of planetary systems* (B. Matthews and J. Graham, eds.), pp. 370-373, International Astronomical Union. ; added MG 29 July 2014
- Maindl T. I., et al. (2013) *Astron. Notes*, 334, 996.
- Mamajek E. E. and Hillenbrand L. A. (2008) *Astrophys. J.*, 687, 1264-1293.
- Marley M. S., et al. (2013) In: *Comparative Climatology of Terrestrial Planets* (S. Mackwell, M. Bullock, and J. Harder, eds.), University of Arizona Press, Tucson, AZ.
- Mestel L. (1968), *Mon. Not. Roy. Astron. Soc.*, 138, 359-391.
- Minton D. A. and Malhotra R. (2007) *Astrophys. J.*, 660, 1700-1706.
- Mischna M. M., et al. (2000) *Icarus*, 145, 546-554.
- Mischna M. A., et al. (2013) *J. Geophys. Res. (Planets)*, 118, 560-576.
- Mizuno H. (1980) *Prog. Theor. Phys.*, 64, 544-557.
- Mizuno H., et al. (1978) *Prog. Theor. Phys.*, 60, 699-710.
- Montési L. G. J. and Zuber M. T. (2003) *J. Geophys. Res.-Planets*, 108, 2/1-25, CiteID 5048.
- Morbidelli A. (2013) In *Planets, Stars and Stellar Systems* (T. D. Oswalt, L. M. French, and P. Kalas), pp 63-109. Springer Science+Business Media, Dordrecht.
- Morbidelli A., et al. (2000) *Meteoritics & Planet. Sci.*, 35, 1309-1320.
- Morbidelli A., et al. (2007) *Astron. J.*, 134, 1790-1798.
- Mordasini C., et al. (2012) *Astron. & Astrophys.*, 547, A112.
- National Academy of Sciences (2007) *The Limits of Organic Life in Planetary Systems*, National Acad. Sci., Washington, DC.
- O'Brien D. P., et al. (2006) *Icarus*, 184, 39-58.
- Osten R. A., et al. (2010) *Astrophys. J.*, 721, 785-801.
- Parker E. N. (1958) *Astrophys. J.*, 128, 664-675.
- Paynter D. J. and Ramaswamy, V. (2011) *J. Geophys. Res.*, 116, D20302.
- Penz T., et al. (2008) *Planet. Space Sci.*, 56, 1260-1272.
- Pepe F., et al. (2011) *Astron. Astrophys.*, 534, id.A58.
- Pierrehumbert R. and Gaidos E. (2011) *Astrophys. J.*, 734, id L13.
- Pilat-Lohinger E., et al. (2008) *Astrophys. J.*, 681, 1639-1645.
- Pizzolato N., et al. (2003) *Astron. Astrophys.*, 397, 147-157.
- Pollack J. B., et al. (1996) *Icarus*, 124, 62-85.
- Postawko S. E. and Kuhn W. R. (1986) *J. Geophys. Res.*, 91, 431-438.
- Preusse S., et al. (2005) *Astron. Astrophys.*, 434, 1191-1200.
- Rafikov R. R. (2006) *Astrophys. J.*, 648, 666-682.
- Ramirez R. M., et al. (2014) *Nature Geosci.*, 7, 59-63.
- Rauer H., et al. (2011) *Astron. Astrophys.*, 529, id.A8.
- Raymond S. N., et al. (2004) *Icarus*, 168, 1-17.
- Raymond S. N., et al. (2007) *Astrobiol.*, 7, 66-84.
- Raymond S. N., et al. (2009) *Icarus*, 203, 644-662.
- Reiners A. and Christensen U. R. (2010) *Astron. Astrophys.*, 522, idA13.
- Reinhard C. T. and Planavsky N. J. (2011) *Nature*, 474, E1-E2.
- Ribas I., et al. (2005) *Astrophys. J.*, 622, 680-694.
- Ribas I., et al. (2010) *Astrophys. J.*, 714, 384-395.
- Ringwood A. E. (1979) *Origin of the Earth and Moon*. Springer Publishing House, Heidelberg / New York.
- Roberson A., et al. (2011) *Geobiol.*, 9, 313-320.
- Rondanelli R. and Lindzen R. S. (2010) *J. Geophys. Res.*, 115, D02108.
- Rosing M. T., et al. (2010) *Nature*, 464, 744-747.
- Ringwood A. E. (1979) *Origin of the Earth and Moon*. Springer Publishing House, Heidelberg / New York.

- Rossow W. B., et al. (1982) *Science*, 217, 1245-1247.
- Rugheimer S., et al. (2013) *Astrobiol.*, 13, 251-269.
- Rye R., et al. (1995) *Nature*, 378, 603-605.
- Sackmann I.-J. and Boothroyd A. I. (2003) *Astrophys. J.*, 583, 1024-1039.
- Sagan C. and Mullen G. (1972) *Science*, 177, 52-56.
- Sánchez-Lavega A. (2004) *Astrophys. J.*, 609, L87-90.
- Sanz-Forcada J., et al. (2011) *Astron. Astrophys.*, 532, A6.
- Scalo J., et al. (2007) *Astrobiol.*, 7, 85-166.
- Schaefer B. E., et al. (2000) *Astrophys. J.*, 529, 1026-1030.
- Schrijver C. J., et al. (2012) *J. Geophys. Res.*, 117, CiteID A08103.
- Seager S. (2013) *Science*, 340, 577-581.
- Seager S., et al. (2013) *Astrophys. J.*, 777, id.95.
- Segura A., et al. (2005) *Astrobiol.*, 5, 706-725.
- Segura A., et al. (2010) *Astrobiol.*, 10, 751-771.
- Sekiya M., et al. (1980) *Prog. Theor. Phys.*, 64, 1968-1985.
- Sekiya M., et al. (1981) *Prog. Theor. Phys.*, 66, 1301-1316.
- Selsis F., et al. (2008) *Phys. Scripta*, 130, id. 014032.
- Sheeley N. R. Jr., et al. (1997) *Astrophys. J.*, 484, 472-478.
- Sheldon N. D. (2006) *Precambrian Res.*, 147, 148-55.
- Soderblom D. R., et al. (1993) *Astrophys. J.*, 409, 624-634.
- Stern R. A., et al. (1995) *Astrophys. J.*, 448, 683-704.
- Stewart S. T. and Leinhardt Z. M. (2012) *Astrophys. J.*, 751, id 32.
- Telleschi A., et al. (2005) *Astrophys. J.*, 622, 653-679.
- Tian F., et al. (2005) *ApJ*, 621, 1049-1060.
- Tian F., et al. (2008) *J. Geophys. Res.*, 113, E05008.
- Tian F., et al. (2009) *Geophys. Res. Lett.* 36, L02205.
- Tian F., et al. (2010), *Earth Plan. Sci. Lett.*, 295, 412-418.
- Tsiganis K., et al. (2005) *Nature*, 435, 459-461.
- Ueno Y., et al. (2009) *Proc. Nat. Acad. Sci.*, 106, 14784-14789.
- Valley J. W., et al. (2002) *Geology*, 30, 351-354.
- van den Oord G. H. J. and Doyle J. G. (1997) *Astron. Astrophys.*, 319, 578-588.
- Vasquez M., et al. (2013a) *Astron. Astrophys.*, 549, id.A26.
- Vasquez M., et al. (2013b) *Astron. Astrophys.*, 557, id.A46.
- Vidal-Madjar A., et al., (2003) *Nature*, 422, 143-146.
- Volkov A. N. and Johnson R. E. (2013) *Astrophys. J.*, 765, id90.
- von Paris P., et al. (2008) *Planet. Space Sci.*, 45, 1254-1259.
- von Paris P., et al. (2010) *Astron. Astrophys.*, 522, id.A23.
- von Paris P., et al. (2013) *Planet. Space Sci.*, 82, 149-154.
- von Zahn U., et al. (1980) *J. Geophys. Res.*, 85, 7829-7840.
- Walker J. C. G. (1977) *Evolution of the atmosphere*. McMillan, New York.
- Walker J. C. G., et al. (1981) *J. Geophys. Res.*, 86, 9776-9782.
- Walsh K. J., et al. (2011) *Nature*, 475, 206-209.
- Wargelin B. J. and Drake J. J. (2001) *Astrophys. J. Lett.*, 546, L57-L60.
- Watson A. J., et al. (1981) *Icarus*, 48, 150-166.
- Whitmire D. P., et al. (1995) *J. Geophys. Res.*, 100, 5457-5464.
- Wood B. E., et al. (2002) *Astrophys. J.*, 574, 412-425.
- Wood B. E., et al. (2005). *Astrophys. J.*, 628, L143-146.
- Wordsworth R. and Pierrehumbert R. (2013) *Science*, 339, 64-67
- Wordsworth R. D., et al. (2011) *Astrophys. J.*, 733, id.L48.
- Wordsworth R. D., et al. (2010) *Astron. Astrophys.*, 522, id.A22.
- Wuchterl G. (1993) *Icarus*, 106, 323-334.
- Yelle R. V. (2004) *Icarus*, 170, 167-179.
- Yung Y. L. and DeMore W. B. (1999) *Photochemistry of planetary atmospheres*, Oxford University Press, Oxford.
- Zahnle K. J. and Kasting J. F. (1986) *Icarus*, 680, 462-480.
- Zahnle K. J., et al. (1988) *Icarus*, 74, 62-97.
- Zahnle K., et al. (2007) *Space Sci. Rev.*, 129, 35-78.
- Zsom A., et al. (2012) *Icarus*, 221, 603-616.